Carranza-Torres, C. (2021). Computational tools for the analysis of circular failure of rock slopes. Keynote Lecture. In *Proceedings of EUROCK 2021. Mechanics and Rock Engineering from theory to practice*. Turin. Italy. September 21–24, 2021.

A video presentation of this article can be accessed by clicking the link below:

Link to video presentation.

Computational tools for the analysis of circular failure of rock slopes

C Carranza-Torres[1]

[1]Department of Civil Engineering, University of Minnesota, Duluth Campus, USA

E-mail: carranza@d.umn.edu

Abstract. Among other types of failure in slopes created by excavation or filling, circular (also referred to as rotational) type of failure plays an important role in the design and stability analysis of high rock slopes, such as those encountered in deep open pit mines. When a rock slope of significant height involves predominantly one type of jointed rock mass, the scale of the problem is frequently such that the rock mass (intact rock and rock discontinuities) can be regarded as a homogeneous isotropic material. In such case, if the rock slope is unstable and collapse occurs, circular (or rotational) failure as in failed slopes in soils is also observed for the rock slope. One main goal in practical design of deep open pit mines is to determine safe inclination angles for the pit faces to be excavated to avoid failure. Computational tools for quick assessment of the stability conditions, in particular determination of factor of safety and location of the critical circular failure surface, are useful during the preliminary stages of open pit design. Among others, such tools allow the engineer to gain insight in the role that the different variables controlling the problem have in defining the stability conditions for the rock slope. This paper provides first an overview of typical numerical techniques used to assess the stability of high rock slopes. For the case of slopes in rock masses that are assumed to obey the Mohr-Coulomb or the Hoek-Brown failure criteria, the paper discusses how application of transformation rules leads the criteria to be re-casted in dimensionless form, so when these are applied to the solution of slope problems, the results (factor of safety and coordinates that define the location of the critical circular failure surface) can be summarized in dimensionless compact forms. The paper presents then computational tools in the form of dimensionless charts and computer spreadsheets for stability analysis. These are developed from numerical limit equilibrium models that use the mentioned transformation rules. Among others, the computational tools allow the concept of mechanical similarity of rock slopes to be naturally introduced. Finally, the paper presents various rock slope examples that illustrate the use of the computational tools. In these examples, results from limit equilibrium models are also compared with results obtained with full numerical analysis, in particular with finite difference models implementing the shear strength reduction technique.

1. Introduction

The design of rock slopes in deep open pit mines is among the most challenging slope stability problems in the practice of rock mechanics. With the increasing world demand in minerals, open pit mines are getting larger and deeper, and controlling stability of high rock slopes has become a central part of the process of safe design and operation of open pit mines [1, 2, 3, 4].

In the first formal treatment of rock slope stability for open pit mining, Hoek and Bray [5] —see also [6, 7], identified four fundamental modes of failure for rock slopes, namely, *planar*, *wedge*, *toppling* and *circular* mechanisms. The focus of this paper is in the *circular* failure mechanism, which is also referred to as the *rotational* failure mechanism, particularly in the engineering geology and geotechnical engineering literature [8, 9, 10, 11].

With regard to the four fundamental modes of failure for rock slopes introduced by Hoek and Bray [5], at the scale of mine benches (i.e., at the scale that comprises rock walls of 10 to 30 meters high), slope design is controlled by planar, wedge and/or toppling failures mainly. At this scale, the geometrical and mechanical characteristics of the rock discontinuities take relevance over the mechanical properties of the intact rock, and the behavior of the rock is mostly discontinuum. For design and analysis of rock slopes at this scale, kinematic approaches based on stereographic projections or block theory are mostly applicable [12, 13, 14].

At the scale of the full pit depth and/or at the scale of many benches in between access ramps, in the absence of major faults or shear zones, the rock mass is normally regarded as continuum and isotropic, with a shear strength characterized with material models such as the generalized Hoek-Brown failure criterion [15, 16, 17]. At this scale, similar slope stability models developed in the field of soil mechanics —e.g., limit equilibrium methods with assumption of circular (or rotational) failure surfaces— are commonly used to verify the stability of the rock slopes [6, 7, 14]. To illustrate the idea, Figures 1a through 1d show photographs of collapses in large open pit mines at the scale of full or inter-ramp depth —the collapses are documented in [18, 19], [18], [20] and [1], respectively. In all cases, due to the scale of the failure, the rock mass fails resembling typical circular (or rotational) failures observed in failed slopes in soils —even when the collapsed rock mass (or rock fill) may be comprised of rock blocks of the size of a truck!

In mining engineering, slope stability problems are also found outside the pit excavations themselves. Rock without mineralization (referred to as mine waste) and rock with mineralization that is waiting to be processed are commonly stored in the form of waste dumps and stockpiles, respectively. Also, mineral processing plants produce residues called tailings, that are typically stored using containment structures called tailings dams. Many times these dams (or parts of them) are constructed using rock fills (i.e., large rock blocks of waste rock from the pit). The stability of the faces of piles or rock fill dams also poses a design challenge. When the pile or dam is high enough, the material can be treated again as a continuum, using rock mass shear strength models such as the Mohr-Coulomb and/or the Power Law models, applying again slope stability tools developed in the field of soil mechanics (e.g., limit equilibrium and circular failure analysis).

This paper deals with the analysis of stability of high rock slopes in mining, whether the slopes belong to the open pit itself or to a waste dump, stockpile or rock fill dam, at a scale such as that of the slopes shown in Figure 1, when the assumption of continuity can be regarded as valid, and the predominant type of failure is circular or rotational. Certainly, the developments presented in this paper are not restricted to open pit mining applications; the developments also apply to rock slopes in civil engineering applications, and even to slopes in soils, provided the rock/soil can be regarded as homogeneous and isotropic, so the predominant type of failure is circular. Therefore, when not explicitly mentioned, the different methods of analysis and shear strength models to be considered in the reminder of this paper, will assume the mentioned scale and the assumption of continuum behavior of the material. Also, 'circular failure' will be used to signify 'rotational failure', even when the failure surface involved may not be strictly of circular geometry.

As with the case of slopes in soils, the traditional means of quantifying the stability of a rock slope against circular failure is by computation of a scalar factor of safety (*FS*). It is standard practice to define this factor of safety as the ratio of the available shear strength over the required shear stress for equilibrium along the potential failure surface. Whether the stability analysis is deterministic or probabilistic, the design of slopes in the open pit (or in waste dump, stockpile or rock fill dam) is carried out on the condition that the factor of safety of the slope is above a safe threshold value, normally, above the critical value of one —see, for example, [11, 21, 22].

Numerical models generated with various commercial software implementations have become important tools for carrying out stability analyses of high rock slopes in rock mechanics mining. Again, considering the scale of the cases represented in Figure 1, these numerical models allow factors of safety for given rock mass properties and potential circular failure surfaces to be determined. Table 1 provides

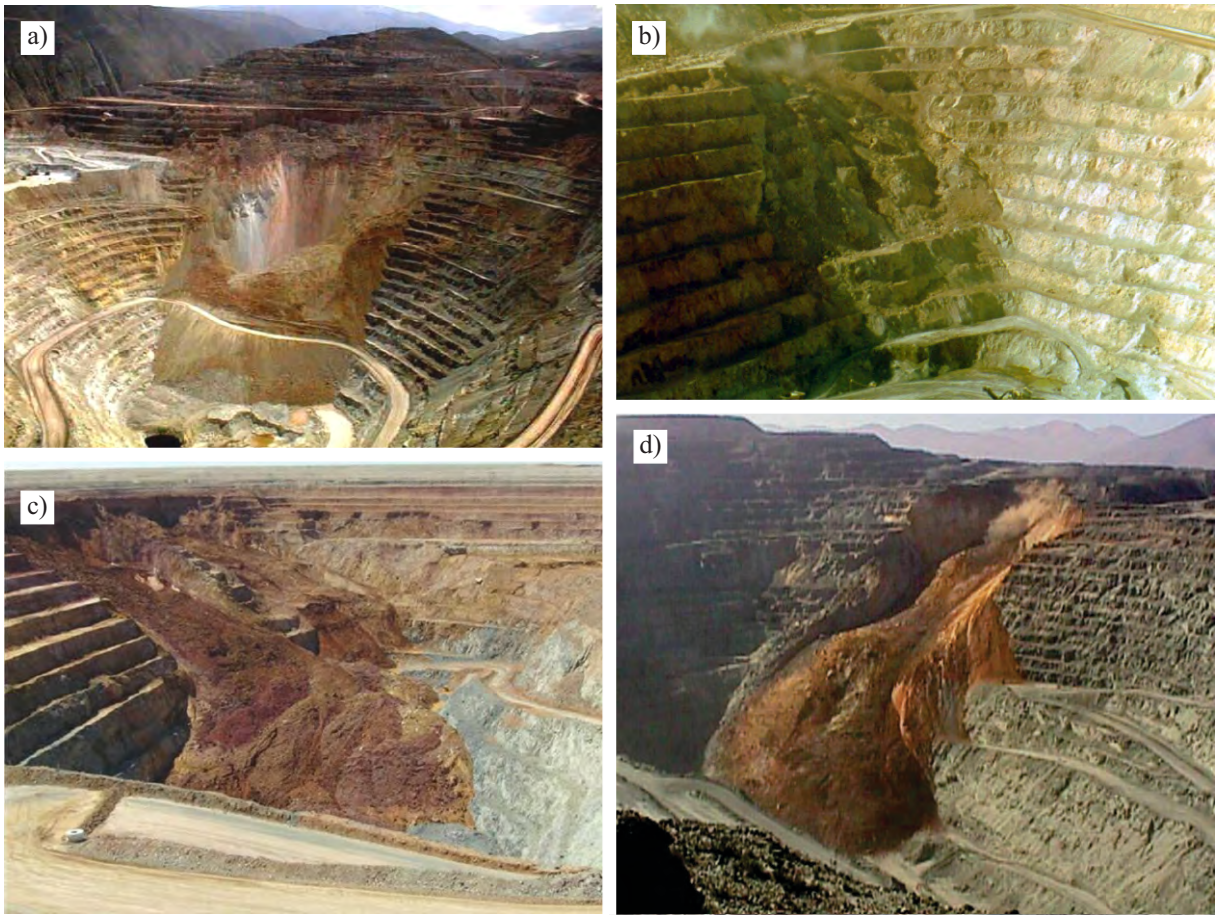

Figure 1. Examples of large rock slope instabilities in open pit mines —after a) [18, 19]; b) [18]; c) [20]; d) [1].

a summary of different methods and examples of commercial software implementations commonly used in the practice of slope stability in rock mechanics mining (there may exist other methods and software implementations which have not been included in Table 1 due to space reasons). As indicated in Table 1, in one end of the spectrum, the *limit equilibrium* method has been the traditional (and still today the most popular) method for analyzing the stability of two-dimensional sections of slope, particularly with the so-called *method of slices* —see, for example, [23, 24, 25, 26]. The advantage of the method is in the simplicity in setting up, computing and interpreting the results. There exist various formulations for computing factors of safety with the method of slices [11, 25]. Among these, the Bishop's formulation [27] is a popular one due to simplicity and low computational demands. In recent years, commercial software implementations of the method of slices allow analysis of stability for slopes in three-dimensions to be done as well.

Referring to Table 1, and on the other side of the spectrum, full numerical analyses, comprising finite element, finite differences and discrete element methods, have gained wide popularity in the design and analysis of high rock slopes in rock mechanics mining. The shear strength reduction technique for computing factors of safety and location of the potential failure surface has become the standard method of slope stability analysis when full numerical methods are applied —see, for example, [28, 29, 30]. The technique allows factors of safety and location of the potential failure surface for both two-dimensional sections of slopes and full three-dimensional slopes to be determined.

To illustrate the application of some of the numerical tools listed in Table 1, Figure 2 shows views of

Table 1. Numerical methods and examples of commercial software implementations typically used in the analysis of stability of high slopes in open pit mines.

Numerical method	Software implementation
Limit equilibrium	GEO05, SLIDE/SLIDE3, SLOPE/W, XSTABL
Finite element	ABAQUS, PLAXIS/PLAXIS3D, RS2/RS3
Finite difference	FLAC/FLAC3D
Distinct element	UDEC/3DEC

numerical models used in the design of rock slopes in the open pit project Rajo Sur in Chile (this open pit mine is located high in the Andes mountains, above El Teniente mine, the largest underground copper mine in the world). A detailed description of the project and the process of designing the rock slopes in the project can be found in [31].

Figure 2a shows the stability analysis results for a section of pit approximately 460 m high in the project. The figure indicates the names of the different rock mass units, the position of the phreatic surface and the resulting factor of safety and critical failure surface obtained with the limit equilibrium method, as implemented in software SLIDE [32]. According to SLIDE, the factor of safety for the slope results to be $FS = 1.42$. Figure 2b shows the analysis of stability of the same section of slope, using the finite difference method, as implemented in the software FLAC [33]. The figure represents contours of scaled maximum shear strain rate which are commonly used to visualize the development of the shear failure surface (in the figure, the title 'scaled shear strain' of the legend refers to the square root of the second invariant of the deviatoric strain rate, that has been scaled, dividing it by the maximum value of shear strain rate in the model at that stage). Figure 2b indicates that the factor of safety obtained with the shear strength reduction technique in FLAC results to be $FS = 1.50$. This value and the outline of the critical failure surface defined by the contours of scaled maximum shear strain rate in Figure 2b result similar to those indicated in Figure 2a, corresponding to the limit equilibrium method. Figures 2c and 2d show the analysis of the stability of the full three-dimensional pit done as part of the project. The contours in Figure 2d highlight the region of the pit that is relatively less stable due to the combination of low rock mass quality and steeper rock slopes. Further details about the different models represented in Figure 2, including values of material properties assigned to the rock mass, can be found in [31].

For a relatively complex two-dimensional rock slope section like that represented in Figures 2a and 2b, a *preliminary* estimation of factor of safety and location of critical failure surface could have been done quickly based on a simplified version of the original slope section. Such simplified version would assume the face to be planar and the rock mass to be homogenous (i.e., modelled as a single lithological unit), and with the rock mass properties defined, for example, as weighted averages of the corresponding properties for the different units cutting the original rock slope.

Figure 3a represents an example of one (of possibly others) simplified version(s) of the rock slope in Figures 2a and 2b. The angle of inclination of the slope assuming a planar face and the mechanical properties for a representative homogeneous rock mass are indicated in the figure —the inclination angle of the slope has been assumed to be the mean inclination angle of the slope section in Figure 2a, while the Mohr-Coulomb strength properties have been estimated as weighted averages of those corresponding to the three units cutting the slope face in Figure 2a, as reported in [31]. The resulting factors of safety and locations of the potential failure surfaces for the simplified rock slope section are indicated in Figure 3 — Figure 3a shows results obtained with the limit equilibrium software SLIDE, while Figure 3b shows those obtained with the finite difference software FLAC. The results shown in Figure 3 are not too different from those obtained for the full complex rock slope in Figures 2a and 2b, supporting the idea that a quick preliminary estimation of stability conditions could have been obtained with simplified slope models.

Simplified models such as those represented in Figure 3 are useful in the preliminary design of rock

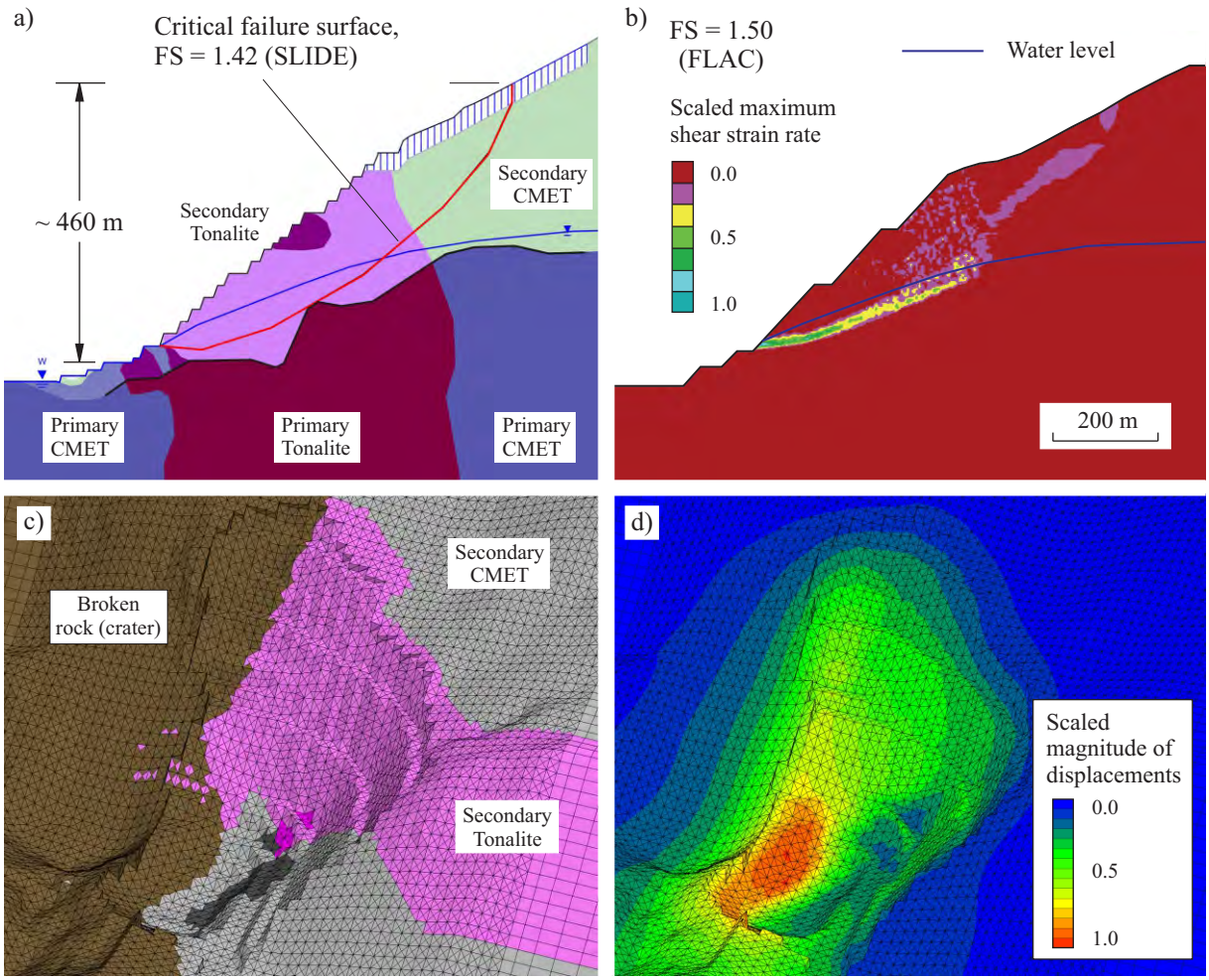

Figure 2. Numerical models applied to slope stability analysis in a large open pit mine project —after [31].

slopes in open pit mines. Among others, these models allow the design engineer to quickly establish the dependence of input variables (e.g., planned overall slope angle and depth, and rock mass properties) on output results (i.e., factor of safety and location of critical failure surface). This is a required process in the preliminary design stage, due to the intrinsic variability and uncertainty of the input variables, particularly, the rock mass properties.

Stability results from simplified slope models as represented in Figure 3, have been traditionally presented in the form of dimensionless charts; this has been the case since the early developments of slope stability analyses in soil mechanics —see [11] for a historical list of publications presenting dimensionless charts for slope stability analysis. In the modern practice of rock mechanics mining, these results can also be made available in the form of computer spreadsheets, for example, written for the software EXCEL [34]. This can be accomplished by developing spreadsheets that include table-lookup algorithms to search results in a digital database of already computed cases of simplified slopes as in Figure 3.

The author of this paper considers that engineers involved in the design of open pit slopes (as well as students being trained in rock slope engineering) should not have to resort to acquiring and using complex commercial applications for slope stability analysis, as listed in Table 1, to analyze dependence

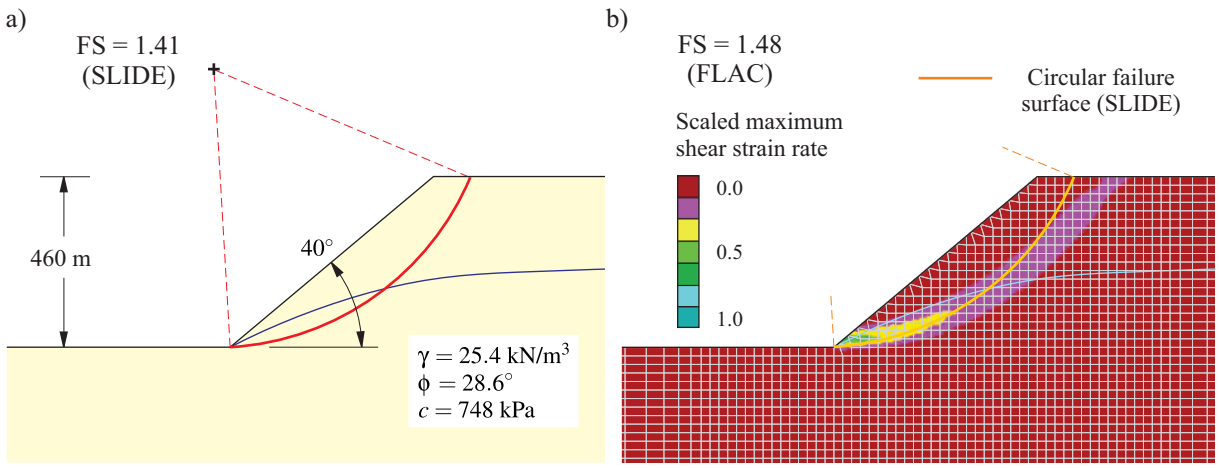

Figure 3. Stability results obtained from a) limit equilibrium and b) finite difference models for a simplified version of the slope sections shown in Figures 2a and 2b.

of variables on slope stability mainly through simplified models as in Figure 3. This is because with the computer power existing nowadays, dimensionless representations and EXCEL spreadsheet algorithms of the type mentioned above, for the analysis of stability of simple slopes, can be developed relatively easily using dimensional analysis, and by computing properly selected slope cases with any of the software tools listed in Table 1.

The main objective of this paper is to discuss the development and application of a series of computational tools as described above, to quickly analyze the stability of simplified slopes like those in Figure 3, for rock masses assumed to obey the Mohr-Coulomb and the Hoek-Brown shear failure criteria. These computational tools have been presented in three recent publications written by the author and colleagues [35, 36, 37]. As discussed in these publications, the computational tools for slopes in Mohr-Coulomb material, in particular, are based on dimensionless 'circular' charts originally proposed by Hoek and Bray [5] —see also [6, 7]. The recent publications [35, 36, 37] are accompanied by EXCEL spreadsheets that include the mentioned table-lookup search algorithms of slope results, computed with limit equilibrium models. The publications and corresponding EXCEL spreadsheets, to be referred to throughout the next sections of this paper, can be freely downloaded using the internet links provided in Section 6, at the end of this paper.

2. Transformation of shear strength models for rock

An important aspect of the development of the computational tools discussed at the end of last section is in defining transformation rules for the variables involved in the problem. Application of such transformations allows the number of slope cases to evaluate for the development of the computational tools to be reduced. As it will be shown in later sections in this paper, use of the transformation rules also allows compact representation of results (i.e., factor of safety and location of circular failure surface) to be obtained.

Transformation of two common shear strength models will be considered separately in this section: *i)* the Mohr-Coulomb model; and *ii)* the Hoek-Brown model.

As mentioned in the introduction Section 1, the Mohr-Coulomb shear strength model has applications in slopes in predominantly granular material (including rock fills), and in slopes in very weak rocks (including, of course, soils). The Hoek-Brown failure criterion has applications in slopes in jointed rock masses, when the scale of the problem is such that the assumption of continuity is valid. It is also possible to compute equivalent Mohr-Coulomb properties for a rock mass that has been characterized in terms of

Hoek-Brown properties, using equations presented in [38]. This equivalence will be illustrated later on with an example in Section 4.

2.1. Transformation of the Mohr-Coulomb model

The Mohr-Coulomb shear strength failure criterion is written as follows —see, for example, [12, 39, 40]

$$\tau_s = \sigma_n \tan\phi + c \tag{1}$$

where σ_n and τ_s are the normal and shear stresses on the failure plane, ϕ is the internal friction angle, and c is the cohesion.

The transformation of the Mohr-Coulomb shear strength model will be presented and illustrated here with the analysis of direct shear tests carried out for different types of rock fill, as reported in [41, 42, 43]. Although the shear strength of a rock fill is commonly characterized by a non-linear Power Law model (that will predict null cohesion for a non-cemented rock fill), for illustration purposes, a linear Mohr-Coulomb model will be used here.

Table 2a lists direct shear test results (normal stresses $\sigma_{n,i}$, and shear stresses $\tau_{s,i}$) for three types of rock fill, designated as RF-1, RF-2 and RF-3 in the table —these are identified as 'Mica granitic gneiss', 'El infiernillo diorite' and 'Argillite at Pyramid dam' in [43]. Assuming that for each rock fill type the pairs $\sigma_{n,i}$ and $\tau_{s,i}$ obey the Mohr-Coulomb failure criterion given by equation (1), best fit Mohr-Coulomb envelopes have been computed using linear regression analysis. The resulting values of cohesion and internal friction angle for the rock fills RF-1, RF-2 and RF-3 are listed at the bottom of Table 2a (note that the computed cohesion is actually an apparent cohesion, and it is the result of linearizing a non-linear shear strength envelope that passes through the origin of the σ_n vs τ_s diagram). Coefficients of determination (r^2) for each of the best fit envelopes are also reported in Table 2a, with these values being close to one, suggesting a quite good fit.

Figure 4a represents the pairs $(\sigma_{n,i}, \tau_{s,i})$ and the best fit Mohr-Coulomb shear strength envelopes for the three different rock fills in Table 2a. As these correspond to different rock types with different granulometry, there are three distinct failure envelopes in the figure.

The transformation rule for the Mohr-Coulomb shear strength model involves dividing both shear and normal stresses by the cohesion, and multiplying the normal stress by the tangent of the internal friction angle, i.e.,

$$S_n = \frac{\sigma_n}{c}\tan\phi; \qquad T_s = \frac{\tau_s}{c} \tag{2}$$

In the equations above, capital letters have been used to signify transformed stresses.

When stresses have been transformed as in equations (2), it can be readily seen that the Mohr-Coulomb shear strength criterion given by equation (1) takes the following dimensionless simple form

$$T_s = S_n + 1 \tag{3}$$

The transformed pairs $S_{n,i}$ and $T_{s,i}$ for the rock fills RF-1, RF-2 and RF-3, using the respective best fit values of internal friction angle and apparent cohesion, are listed in Table 2b and they are represented graphically in Figure 4b, together with the transformed version of Mohr-Coulomb failure envelope given by equation (3). From Figure 4b it can be seen that all three different types of rock fill obey now a single failure envelope. The 'unified' dimensionless Mohr-Coulomb shear strength envelope given by equation (3), which encompasses all possible Mohr-Coulomb shear failure envelopes (i.e., envelopes for every possible combination of the Mohr-Coulomb parameters ϕ and c in equation 1), will be incorporated into the analysis of stability of slopes in Section 3.1. Use of this unified failure model will bring the advantages mentioned earlier on, when developing the computational tools for slopes involving Mohr-Coulomb rock masses or rock fills.

Table 2. a) Normal and shear stresses at failure, and best fit Mohr-Coulomb properties obtained from direct shear testing of three types of rock fill; b) Transformed normal and shear stresses at failure.

a)

Test	$(\sigma_{n,i}, \tau_{s,i})$ [MPa] RF-1		RF-2		RF-3	
1	0.15	0.18	0.31	0.32	0.31	0.39
2	0.73	0.55	0.79	0.65	1.60	1.41
3	1.51	1.02	1.61	1.21	2.98	2.38
4	2.60	1.65	2.70	1.89	3.93	3.00
5	3.82	2.38				
c [MPa]	0.105		0.129		0.206	
ϕ [°]	30.8		33.31		35.77	
r^2 [-]	1.000		1.000		0.999	

b)

Test	$(S_{n,i}, T_{s,i})$ [-] RF-1		RF-2		RF-3	
1	0.85	1.71	1.58	2.49	1.08	1.89
2	4.13	5.21	4.04	5.05	5.59	6.83
3	8.54	9.67	8.23	9.41	10.40	11.53
4	14.70	15.64	13.80	14.69	13.72	14.54
5	21.59	22.56				

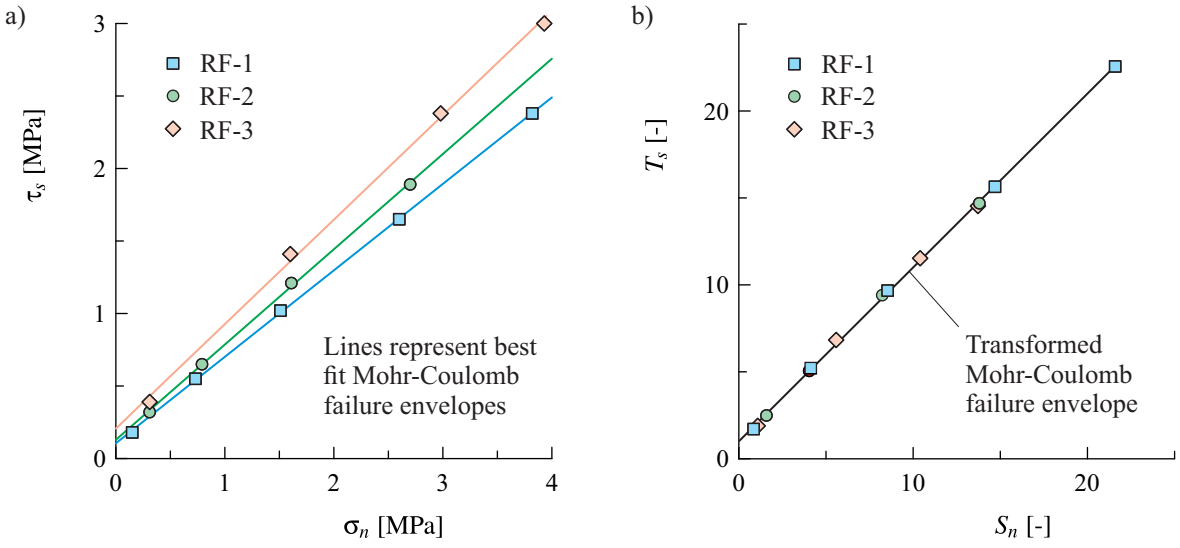

Figure 4. Graphical representation of the direct shear testing results for the three types of rock fill in Table 2. a) Original and b) transformed representations of normal and shear stresses at failure.

2.2. Transformation of the Hoek-Brown model

The generalized Hoek-Brown failure criterion for rock masses is written as follows —see, for example, [15, 16, 17]

$$\sigma_1 = \sigma_3 + \sigma_{ci}\left(m_b\frac{\sigma_3}{\sigma_{ci}} + s\right)^a \tag{4}$$

where σ_3 and σ_1 are the minor and major principal stresses at failure, σ_{ci} is the uniaxial compressive strength of the intact rock, and m_b, s and a are dimensionless parameters characterizing the strength of the rock mass. According to the latest versions of the Hoek-Brown failure criterion [17, 38], the parameters m_b, s and a are computed based on the following equations

$$m_b = m_i \exp\left(\frac{\mathrm{GSI}-100}{28-14\mathrm{D}}\right) \tag{5}$$

$$s = \exp\left(\frac{\mathrm{GSI}-100}{9-3\mathrm{D}}\right) \tag{6}$$

$$a = \frac{1}{2} + \frac{1}{6}\left(e^{-\mathrm{GSI}/15} - e^{-20/3}\right) \tag{7}$$

In equation (5), m_i is a parameter obtained from triaxial testing of intact rock samples. In equations (5) through (7), GSI is the geological strength index, a scalar value between 0 and 100 estimated from the degree of jointing and condition of the joint surfaces of the rock mass in the field (with increasing values of GSI corresponding to increasing quality of the rock mass). In equations (5) and (6), D is the disturbance factor, another scalar value between 0 and 1, estimated based on the expected damage of the rock mass surrounding the slope —i.e., in the case of slopes in open pits, estimated based on the quality of blasting (with increasing values of D corresponding to decreasing blasting quality). For the case of slopes, this factor is only applied to the damaged rock immediately behind the excavated surface, and it has no impact on the properties of the overall rock mass where a deep seated failure surface would be located.

It is important to note too that the classical Hoek-Brown failure criterion for intact rock can be obtained by making $m_b = m_i$, $s = 0$ and $a = 0.5$ in equation (4) —or equivalently, GSI = 100 and D = 0 in equations (5) through (7)— yielding

$$\sigma_1 = \sigma_3 + \sigma_{ci}\sqrt{m_i\frac{\sigma_3}{\sigma_{ci}} + 1} \tag{8}$$

For the case of slopes considered in this paper, the generalized Hoek-Brown failure criterion given by equation (4) has to be expressed in terms of normal and shear stresses on the failure plane, as done for the case of the Mohr-Coulomb failure criterion in the previous section. Balmer's equations [44] allow the relationship between τ_s and σ_n to be found —the procedure is explained in [45]. For simplicity, the relationship will be written here in the following generic form

$$\tau_s = f_{HB}\left(\sigma_n, \sigma_{ci}, m_b, s, a\right) \tag{9}$$

In equation (9), f_{HB} represents a function of the independent variable σ_n, that according to equation (4) also depends on the variables σ_{ci}, m_b, s and a.

The transformation of the Hoek-Brown failure criterion will be presented and illustrated next with the analysis of actual triaxial tests carried out on intact rock specimens of andesite, corresponding to a single lithological unit in an open pit mining project.

The three columns on the left of Table 3 list triaxial test results for the intact rock samples. These are the columns labelled as $\sigma_{3,i}^{\mathrm{IR}}$ and $\sigma_{1,i}^{\mathrm{IR}}$, respectively (the superscript 'IR' denoting intact rock), corresponding to the applied confining stresses and the measured axial stress at failure, respectively.

Table 3. Minor and major stresses at failure, and best fit Hoek-Brown properties obtained from triaxial testing of intact rock —columns $\sigma_{3,i}^{IR}$ and $\sigma_{1,i}^{IR}$. Computed minor and major stresses at failure for rock masses of decreasing quality —columns $\sigma_{3,i}$ and $\sigma_{1,i}$.

Test	$(\sigma_{3,i}^{IR}, \sigma_{1,i}^{IR})$ [MPa] Intact rock		$(\sigma_{3,i}, \sigma_{1,i})$ [MPa] GSI = 100		GSI = 80		GSI = 40	
1	0.00	120.50	0.00	120.50	0.00	39.67	0.00	4.30
2	5.00	161.80	5.00	161.80	5.00	86.39	5.00	40.17
3	10.50	198.40	10.50	198.40	10.50	119.90	10.50	60.69
4	15.00	225.10	15.00	225.10	15.00	142.76	15.00	74.65
5	20.20	263.00	20.20	263.00	20.20	172.61	20.20	92.52
6	25.40	283.60	25.40	283.60	25.40	190.44	25.40	103.96
σ_{ci} [MPa]	119.34							
m_i [-]	17.47							
m_b [-]			17.47		8.55		2.05	
s [-]			1.0000		0.1084		0.0013	
a [-] (assumed)			0.5		0.5		0.5	

A best fit intact rock Hoek-Brown failure envelope, defined by equation (8), has been computed for the triaxial test results using the software ROCDATA [46]. The resulting values of the parameters σ_{ci} and m_i are listed at the bottom of the columns $\sigma_{3,i}^{IR}$ and $\sigma_{1,i}^{IR}$ in Table 3.

Figure 5a represents the pairs $\sigma_{3,i}^{IR}$ and $\sigma_{1,i}^{IR}$ in Table 3 and the corresponding best fit Hoek-Brown shear strength envelope. No correlation coefficient has been computed for the non-linear fit of the intact rock test results, but visual inspection of the distances of points representing the triaxial tests and the corresponding best fit envelope in Figure 5a suggests a good fit.

Because the objective of this section is to illustrate the transformation of the generalized Hoek-Brown failure criterion given by equation (4) (i.e., rather than that of the Hoek-Brown failure criterion for intact rock given be equation 8), the triaxial test results represented in Figure 5a are used to compute the strength of hypothetical rock masses, involving the same intact rock. The rock masses are assumed to be of decreasing quality, characterized by arbitrarily chosen values of geological strength index GSI equal to 100, 80 and 40. The minor and major principal stresses for the rock masses are listed in the remaining columns of Table 3 —see columns labelled as $\sigma_{3,i}$ and $\sigma_{1,i}$. These principal stresses have been computed based on the triaxial test results using equations (4) through (6). The resulting values of the Hoek-Brown parameters m_b and s computed with equations (5) and (6) are listed at the bottom of the table. Also, for reasons to be explained later on in this section, the parameter a in the Hoek-Brown failure criterion given by equation (4) is assumed to be equal to 0.5. With regard to the values of principal stresses for rock masses listed in Table 3, and as mentioned earlier on, the case of GSI = 100 corresponds to a rock mass of excellent quality for which the strength correspond to that of the intact rock; for this reason, the values of principal stresses for the rock mass GSI = 100 in Table 3, coincide with the values of principal stresses from the intact rock triaxial tests. Figure 5b represents the pairs $\sigma_{3,i}$ and $\sigma_{1,i}$ and the corresponding Hoek-Brown shear strength envelopes for the rock masses of decreasing quality in Table 3.

Using the Balmer's equations mentioned earlier on, the failure envelopes and test results for the rock masses represented in Figure 5b, can also be represented in terms of normal and shear stresses on the failure plane. The columns labelled as $\sigma_{n,i}$ and $\tau_{s,i}$ in Table 4a list the values of normal and shear stresses on the failure plane for the different rock masses, after application of Balmer's equations, as explained in [45]. These pairs of values, together with the corresponding Hoek-Brown failure envelopes expressed in terms of normal and shear stresses (computed with equation 9), are represented Figure 6a.

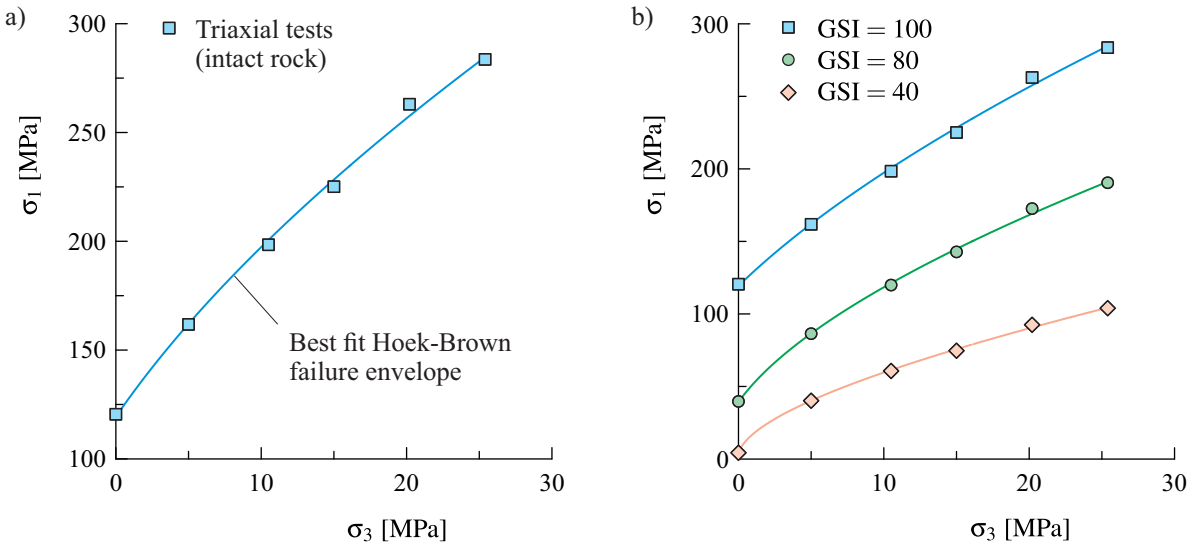

Figure 5. Graphical representation of minor and major principal stresses at failure for a) intact rock and b) rock masses of decreasing quality, listed in Table 3.

Since the interest in this paper is in the analysis of slope stability problems, only the transformation for the Hoek-Brown failure criterion expressed in terms of normal and shear stresses, as in equation (9), will be discussed here —the transformation also applies to the Hoek-Brown failure criterion expressed in terms of principal stresses, as in equation (4), and the reader interested in the full details of the transformation is referred to other publications by the author, e.g., [47, 48].

The transformation rule presented next assumes that the parameter a in equation (4) is equal to 0.5, which is a reasonable assumption for most moderate to good rock mass qualities, with values of geological strength index GSI > 40 (an application example presented later on in Section 4, that considers a slope in a very weak rock mass, shows the limitations of the assumption). The transformation rule involves dividing both shear and normal stresses by the term $m_b\,\sigma_{ci}$, and adding to the normal stress the term s/m_b^2, i.e.,

$$S_n = \frac{\sigma_n}{m_b\,\sigma_{ci}} + \frac{s}{m_b^2}; \qquad T_s = \frac{\tau_s}{m_b\,\sigma_{ci}} \tag{10}$$

As for the case of the transformation of the Mohr-Coulomb failure criterion discussed in Section 2.1, capital letters are used in equations (10) to signify transformed stresses.

It can be shown that when stresses have been transformed as in equations (10), the generalized Hoek-Brown failure criterion given by equation (9) can be expressed in the following dimensionless generic form [36, 45],

$$T_s = F_{HB}\,(S_n) \tag{11}$$

The transformed pairs $S_{n,i}$ and $T_{s,i}$ for the different rock masses, computed with equations (10), are listed in Table 4b and they are represented graphically in Figure 6b, together with the transformed version of Hoek-Brown failure envelope given by equation (11). From Figure 6b it can be seen that all four rock masses obey now a single shear failure envelope.

The 'unified' dimensionless Hoek-Brown shear strength envelope given by equation (11), which encompasses all possible Hoek-Brown shear failure envelopes (i.e., envelopes for every possible combination of the Hoek-Brown parameters σ_{ci}, m_b and s, with $a = 0.5$), will be incorporated into the analysis of stability of slopes in Section 3.2. Use of this 'unified' failure model will bring the advantages mentioned at the beginning of this section, for the development of the computational tools for slopes involving rock masses that satisfy the Hoek-Brown shear failure criterion.

Table 4. Computed a) normal and shear stresses and b) transformed normal and shear stresses at failure for the rock masses in Table 3.

a)

Test	$(\sigma_{n,i}, \tau_{s,i})$ [MPa] GSI = 100		GSI = 80		GSI = 40	
1	11.12	35.02	2.62	9.90	0.14	0.76
2	23.18	50.17	14.87	26.55	11.44	13.59
3	35.90	63.97	27.25	39.25	22.05	21.07
4	45.98	74.10	36.89	47.91	30.13	25.89
5	57.34	88.05	47.62	58.92	39.05	31.83
6	68.45	96.12	58.03	65.66	47.64	35.38

b)

Test	$(S_{n,i}, T_{s,i})$ [-] GSI = 100		GSI = 80		GSI = 40	
1	8.61E-3	1.66E-2	4.05E-3	9.60E-3	8.69E-4	3.09E-3
2	1.44E-2	2.41E-2	1.61E-2	2.61E-2	4.71E-2	5.57E-2
3	2.05E-2	3.10E-2	2.82E-2	3.89E-2	9.04E-2	8.71E-2
4	2.53E-2	3.61E-2	3.76E-2	4.76E-2	1.24E-1	1.07E-1
5	3.08E-2	4.14E-2	4.81E-2	5.65E-2	1.60E-1	1.28E-1
6	3.61E-2	4.63E-2	5.83E-2	6.46E-2	1.95E-1	1.45E-1

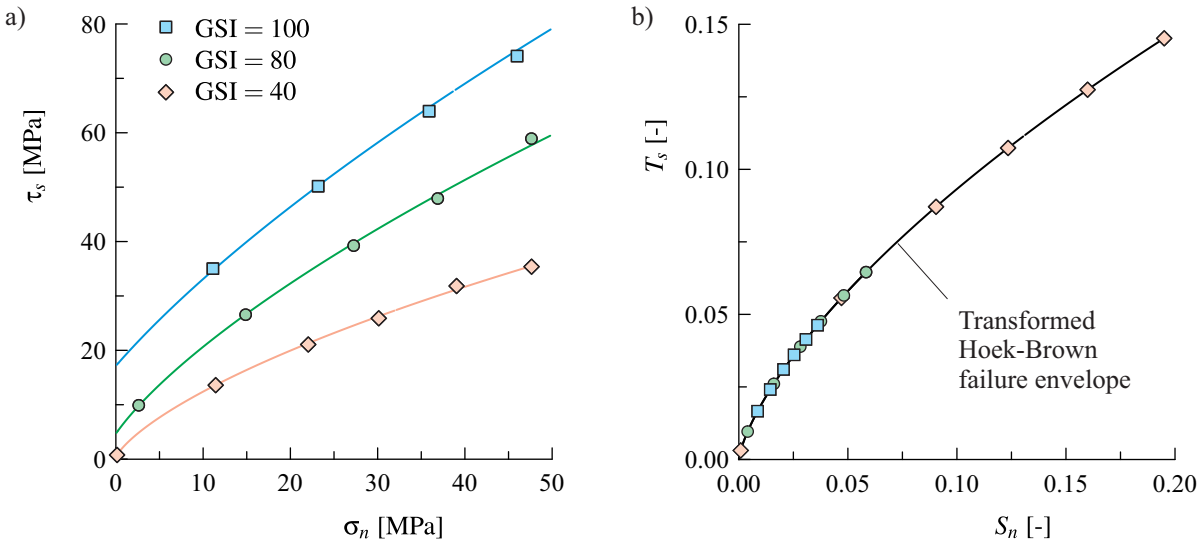

Figure 6. Graphical representation of normal and shear stresses at failure in Table 4. a) Original and b) transformed representations.

3. Circular failure analysis for slopes

The rock slope problem considered in this paper is shown in Figure 7. It involves a two dimensional section of slope of inclination angle α and height H, excavated in an isotropic, homogeneous, dry rock mass of unit weight γ. As discussed already in Section 1 (see Figure 3), the simplified slope model assumes a planar face, so the benches and ramps that are found in open pit slopes are not explicitly considered. The rock mass is assumed to satisfy either the Mohr-Coulomb failure criterion or the Hoek-Brown failure criterion, as discussed already in Section 2. Figure 7 also lists the material properties needed for the application of both Mohr-Coulomb and Hoek-Brown failure models.

Referring to Figure 7, the origin of a system of cartesian coordinates (x,y) is assumed to be located at the *toe* of the slope (point O in the figure). When the shear strength of the rock mass is affected by the factor of safety, the slope is assumed to be at a limit state of equilibrium with a critical (assumed) *circular* failure surface of radius R and center of coordinates x_c and y_c (point C in Figure 7). The starting point of the failure surface (point A in the figure) has coordinates x_A and y_A, while the ending point of the failure surface (point B in the figure) has coordinates x_B and y_B. To simplify the problem, no explicit tension crack is considered for the failure surface. This means that when the center and the starting point of the circular failure surface have been determined, the full circular surface can be defined (e.g., the radius of the circular surface and the position of the ending point of the circular failure surface can be computed based on the coordinates of points C and A in Figure 7).

It must be emphasized that the slope problem in Figure 7 involves a homogeneous rock mass, and no distinction is made for the rock mass immediately (i.e., a few meters) behind the excavation surface. For slopes in large open pit mines, this rock mass is normally damaged due to blasting, and when the rock mass is assumed to obey the Hoek-Brown failure criterion, it has to be assigned a disturbance factor (D) different from zero —see, for example, [17, 49]. In this study, when the Hoek-Brown shear strength model is used, it is assumed that a unique value of D applies to the whole rock mass.

For solving the problem in Figure 7, the most common definition of *factor of safety* (*FS*) will be adopted. This states that the factor of safety is the ratio of the shear strength of the rock mass and the shear stress required for equilibrium on the failure surface —see, for example, [11, 23, 26].

The computational tools to be presented next allow estimation of factor of safety and scaled coordinates of points that define the circular failure surface in Figure 7 —in particular, the scaled coordinates x_c/H, y_c/H, x_A/H, and y_A/H. As mentioned previously, based on the scaled coordinates of points C and A in Figure 7, the scaled radius of the critical failure surface can be computed as follows

$$\frac{R}{H} = \sqrt{\left(\frac{x_c}{H} - \frac{x_A}{H}\right)^2 + \left(\frac{y_c}{H} - \frac{y_A}{H}\right)^2} \tag{12}$$

The computational tools for solving the slope problem in Figure 7 are presented in the following two sections. These deal with slopes in rock masses (or rock fills) that satisfy the Mohr-Coulomb failure criterion and the Hoek-Brown failure criterion, respectively.

3.1. Slopes in rock masses or rock fills that satisfy the Mohr-Coulomb failure criterion

As previously stated in Section 1, the analysis of rock slopes to be presented here is based on dimensionless charts for circular failure that were originally presented in the classical book on rock slopes by Hoek and Bray [5]. The dimensionless variables and range of variables used in the construction of the dimensionless representations are not be exactly the same as originally proposed in [5], but the essence of the analysis is the same.

For the slope problem introduced in Figure 7, a characteristic measure of normal stress can be obtained by multiplying the bulk unit weight of the rock mass or rock fill, γ, and the height of the slope H (for shortness, in the reminder of this section, the word 'rock mass' will be used to mean either rock mass or rock fill). This normal stress can be transformed using the same rule introduced in Section

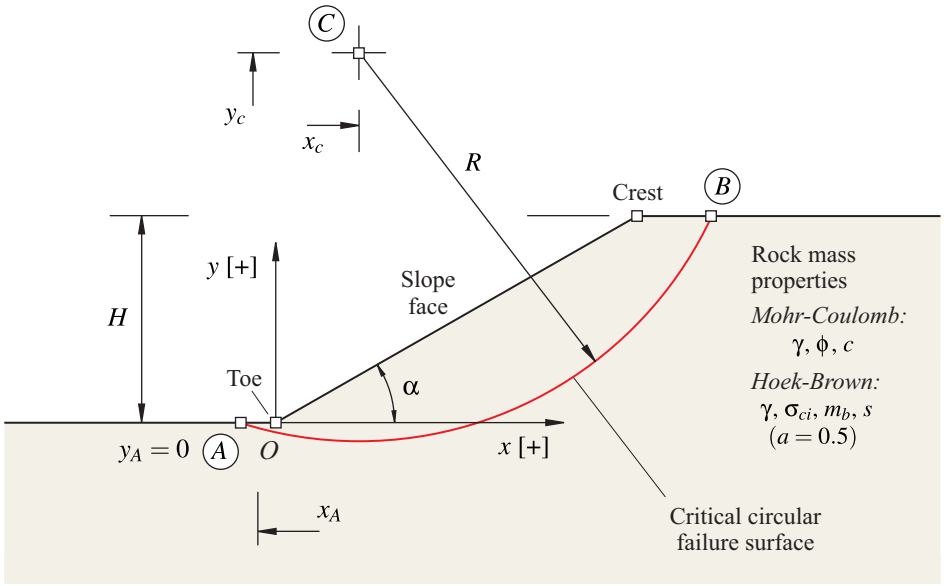

Figure 7. Section of a rock slope in a rock mass that obeys the Mohr-Coulomb or Hoek-Brown failure criteria.

2.1 (equation 2), defining a dimensionless factor to be referred to as X, i.e.,

$$X = \frac{\gamma H \tan\phi}{c} \tag{13}$$

From dimensional analysis, considering the transformed version of the Mohr-Coulomb failure criterion given by equation (3), it can be shown that the factor of safety of the slope in Figure 7 divided by the tangent of the internal friction angle of the rock mass, must depend on the factor X and on the angle of the slope face, α, [5, 35, 50]

$$\frac{FS}{\tan\phi} = f_{FS}(X, \alpha) \tag{14}$$

It can also be shown that the scaled coordinates of the points C and A in Figure 7 that define the position of the critical circular failure surface for the slope, depend on X and α only

$$\frac{x_c}{H} = f_{x_c}(X, \alpha); \qquad \frac{y_c}{H} = f_{y_c}(X, \alpha) \tag{15}$$

and

$$\frac{x_A}{H} = f_{x_A}(X, \alpha); \qquad \frac{y_A}{H} = f_{y_A}(X, \alpha) \tag{16}$$

Equation (12), together with equations (15) and (16), define the scaled radius of the critical failure surface in Figure 7.

In equations (14) through (16), f_{FS}, f_{x_c}, f_{y_c}, f_{x_A} and f_{y_A} represent functions of the independent variables X and α, that can be traced (i.e., constructed by discrete points) by solving a series of slope cases for properly chosen values of these variables. Solution of the slope cases yields general representations of factors of safety and scaled coordinates of the center and starting points of the critical failure surface (and thus the position of the full circular failure surface).

To reconstruct the functions of the variables X and α in equations (14) through (16), the limit equilibrium software SLIDE [32] was employed [35]. A total of 3,402 cases of slopes were evaluated

using the Bishop's method of slices in the software. The input variables in the models were chosen so to obtain 81 equally spaced (in logarithm base-10 scale) slope cases with the factor X between 10^{-2} and 100 (the range of values for X was selected by means of a Monte-Carlo simulation that yielded the expected range of the factor X for typical ranges of values of slope heights, unit weights and Mohr-Coulomb properties encountered in rock engineering). Face inclination angles between 20° and 80°, in increments of 10°, were chosen. The factors of safety and corresponding critical circular failure surfaces were determined for all cases using the 'Autorefine Search' option implemented in the software SLIDE. Full details of the limit equilibrium models used to trace the functions in equations (14) through (16) can be found in [35].

Figure 8 shows the graphical representation of the function f_{FS} in equation (14), as obtained with the software SLIDE. The diagram defines the relationship between the scaled factor of safety $FS/\tan\phi$ (vertical axis) and the dimensionless factor X (horizontal axis), for different face angles α. The small dots on the curves represent the computed limit equilibrium models. In Figure 8, as X decreases, the rock mass is predominantly cohesive, while as X increases, it is predominantly frictional. The figure also shows the positive influence of the cohesion of the rock mass on the factor of safety: for a fixed value of friction angle, the factor of safety increases with the increase in cohesion. It also shows the effect of the slope face angle on the factor of safety: for a fixed value of the factor X, the factor of safety decreases with increase of the face angle. As an example, Point E in Figure 8 represents a slope of inclination angle $\alpha = 50°$ for which $X = 8.473$. The diagram predicts a scaled factor of safety $FS/\tan\phi = 2.14$. Therefore, if the rock mass has an internal friction angle $\phi = 37°$, the factor of safety results to be $FS = 1.61$.

For space reasons, no diagrams for the functions f_{x_c}, f_{y_c}, f_{x_A}, and f_{y_A} in equations (15) and (16) are presented in this paper. Nevertheless, the results needed for constructing graphical representations of these functions (representations similar to that in Figure 8) are included in the EXCEL spreadsheet corresponding to slopes in Mohr-Coulomb rock masses, available for free downloading using the links provided in Section 6. For example, for the same point E included in Figure 8, the EXCEL spreadsheet allows to compute the scaled coordinates of the center of the circular failure surface to be $x_c/H = -0.40$ and $y_c/H = 1.50$, and the scaled coordinates of the starting point of the failure surface to be $x_A/H = yA/H = 0$, this resulting in a scaled radius of the critical failure surface $R/H = 1.55$ —see Figure 7.

A useful computational tool derived from the graphical representation in Figure 8 consists of closed form equations to quickly estimate factors of safety for the slope in Figure 7. The procedure is explained in detail in [35]. The equation for the scaled factor of safety $FS/\tan\phi$ obtained from regression analysis is

$$\frac{FS}{\tan\phi} = \frac{1}{\tan\alpha} + \frac{g_1(\alpha)}{X} + \frac{g_2(\alpha)}{X^{g_3(\alpha)}} \tag{17}$$

where the functions $g_1(\alpha)$, $g_2(\alpha)$ and $g_3(\alpha)$ are computed as follows:

If $\alpha \leq 50°$

$$\begin{aligned} g_1(\alpha) &= 5.524 - 1.222\times10^{-2}(\alpha-50) - 1.569\times10^{-3}(\alpha-50)^2 - 3.097\times10^{-5}(\alpha-50)^3 \\ g_2(\alpha) &= 1.345 - 4.633\times10^{-2}(\alpha-50) + 1.037\times10^{-3}(\alpha-50)^2 + 1.152\times10^{-5}(\alpha-50)^3 \\ g_3(\alpha) &= 3.746\times10^{-1} - 8.727\times10^{-3}(\alpha-50) - 6.384\times10^{-5}(\alpha-50)^2 + 1.808\times10^{-6}(\alpha-50)^3 \end{aligned} \tag{18}$$

If $\alpha \geq 50°$

$$\begin{aligned} g_1(\alpha) &= 5.524 - 4.383\times10^{-2}(\alpha-50) + 1.985\times10^{-4}(\alpha-50)^2 - 5.952\times10^{-6}(\alpha-50)^3 \\ g_2(\alpha) &= 1.345 - 1.035\times10^{-2}(\alpha-50) - 4.092\times10^{-4}(\alpha-50)^2 + 1.044\times10^{-5}(\alpha-50)^3 \\ g_3(\alpha) &= 3.746\times10^{-1} - 7.652\times10^{-4}(\alpha-50) - 2.134\times10^{-4}(\alpha-50)^2 + 4.164\times10^{-6}(\alpha-50)^3 \end{aligned} \tag{19}$$

Equations (17) through (19) allow to reconstruct the different curves in the dimensionless diagram in Figure 8. The equations also recover the solution of factor of safety for an infinite slope, in the case of purely frictional rock mass. Indeed, when X tends to infinity, all different curves in Figure 8 become

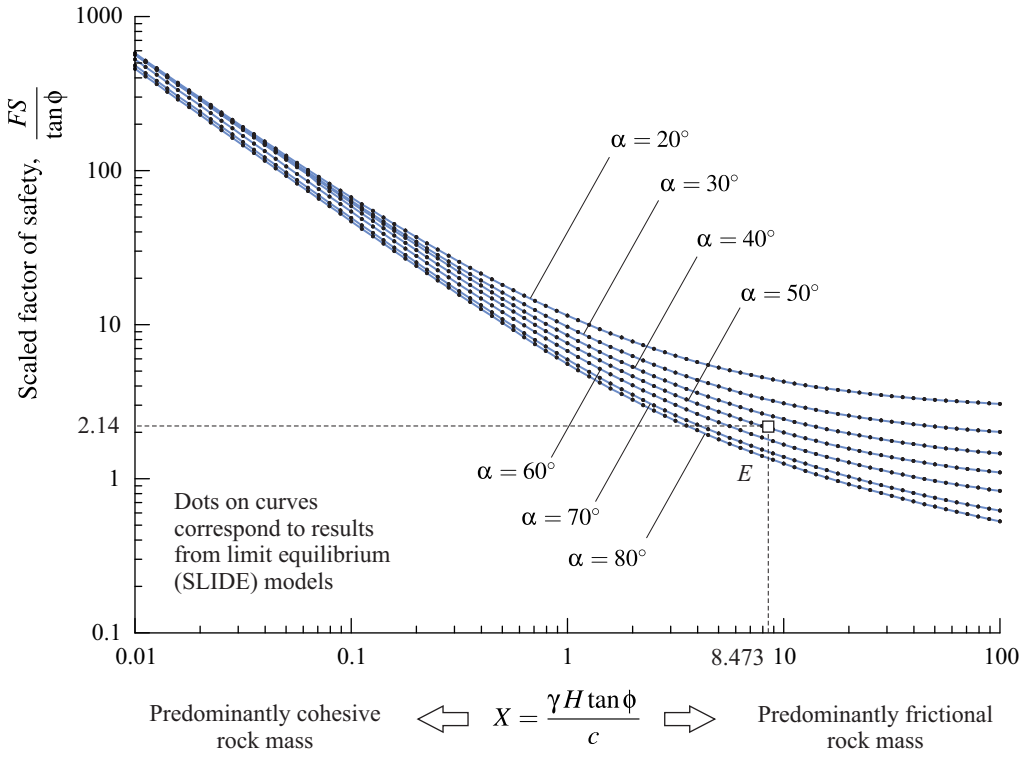

Figure 8. Dimensionless stability diagram for estimation of factor of safety of slopes in rock masses that satisfy the Mohr-Coulomb failure criterion.

asymptotic towards the scaled factor of safety predicted by the analytical solution of an infinite slope in purely frictional Mohr-Coulomb material, i.e., $FS/\tan\phi = 1/\tan\alpha$ —see, for example, [11, 23, 26]. The interested reader is referred to [35] for more details about the equations (17) through (19), including a discussion on the expected differences in values of factor of safety obtained with the equations and with the EXCEL spreadsheet.

The concept of mechanical similarity of slopes, with regard to factor of safety and position of the critical failure surface, arises naturally from the dimensionless functions in equations (14), (15) and (16). The concept will be presented here by means of an example.

Five different cases of slopes, as listed in Table 5a, are considered. At first sight, and disregarding the fact that all slopes have the same inclination angle ($\alpha = 50°$), these correspond to quite different heights and rock mass properties (Case 1 and Case 5 in Table 5a, which correspond to unrealistic slopes of heights 0.3 m and 3,000 m, respectively, are included for illustration purposes only). Nevertheless, according to the last column in Table 5a, all cases are characterized by the same dimensionless factor X (equal to 8.473). Therefore, according to equations (14) through (16), the cases are expected to have the very same values of scaled factor of safety ($FS/\tan\phi$) and scaled coordinates of the different points that form the critical failure surface (i.e., the scaled coordinates of points C, A, etc. in Figure 7). To illustrate this, Table 5b lists the values of scaled factor of safety and scaled coordinates of the center, starting point and radius of the critical failure surface, for all cases, as obtained with equations (14) through (16) using the EXCEL spreadsheet mentioned earlier on. The scaled factor of safety and scaled coordinates of the failure surface listed in Table 5b are the same for all five considered cases, so the slopes are said to be mechanically similar.

The diagram in Figure 9, which is equivalent to the one in Figure 8, further illustrates the concept of mechanical similarity of slopes. In this diagram only three curves corresponding to slope face angles

Table 5. Example of slopes displaying similarity of scaled factor of safety and critical failure surface location —case of Mohr-Coulomb rock masses.

a)

Case	α [°]	H [m]	γ [kN/m^3]	ϕ [°]	c [kPa]	$X = \gamma H \tan\phi / c$ [-]
1		0.3	25	45	8.852E-1	
2		3	19	15	1.803	
3	50	30	24	35	5.95E+1	8.473
4		300	25	37	6.67E+2	
5		3,000	27	8	1.344E+3	

b)

Case	X [-]	$FS/\tan\phi$	x_c/H [-]	y_c/H [-]	x_A/H [-]	y_A/H [-]	R/H [-]
1							
2							
3	8.473	2.14	-0.40	1.50	0.00	0.00	1.55
4							
5							

equal to 30°, 50° and 70° are included. The different sketches above the curves in Figure 9 correspond to slope cases in predominantly cohesive rock masses (characterized by an arbitrarily chosen value $X = 0.05$), cases in typical cohesive-frictional rock masses (arbitrarily chosen value $X = 1$), and cases in predominantly frictional rock masses (arbitrarily chosen value $X = 25$). The sketches show the shape of the critical circular failure surface as obtained with the EXCEL spreadsheet mentioned earlier on. It is seen that when the angle of the slope face is fixed, the average thickness of the critical failure surface depends on the dimensionless factor X only. For this reason, the factor X defined by equation (13) will be referred to as the *similarity factor X* in the reminder of this paper.

Referring also to Figure 9, it should be noticed that all five cases listed in Table 5 plot as point E on the curve corresponding to $\alpha = 50°$ in Figure 9. Therefore, the sketch labelled as E in Figure 9 is representative of the shape of the critical circular failure surface for all five slope cases listed in Table 5.

The concept of mechanical similarity illustrated by the different slope cases in Figure 9 agrees with an observation that dates back to the early developments of limit equilibrium methods for analysis of slope stability in soil mechanics: *slopes in predominantly cohesive soils tend to show deeper critical failure surfaces than those in predominantly frictional soil*. Indeed, it has also been known that for slopes in purely frictional soil, the thickness of the critical failure surface becomes null, as proved by the analytical solution of an infinite slope in cohesionless soil [11, 23, 26, 35].

Finally, the computational tools presented in this section will not be applicable to cases of slopes in rock masses that are characterized as *purely cohesive*. If the internal friction angle of the rock mass is equal to zero, the similarity factor X in equation (13) becomes undetermined. For the case of purely cohesive rock masses, a new set of tools would be required, with the consideration that in the slope problem in Figure 7, the position of a firm horizon beneath the slope (that the failure surface is assumed unable to cut through) will always dictate the extent in depth of the critical failure surface —see, for example, [51, 52, 53].

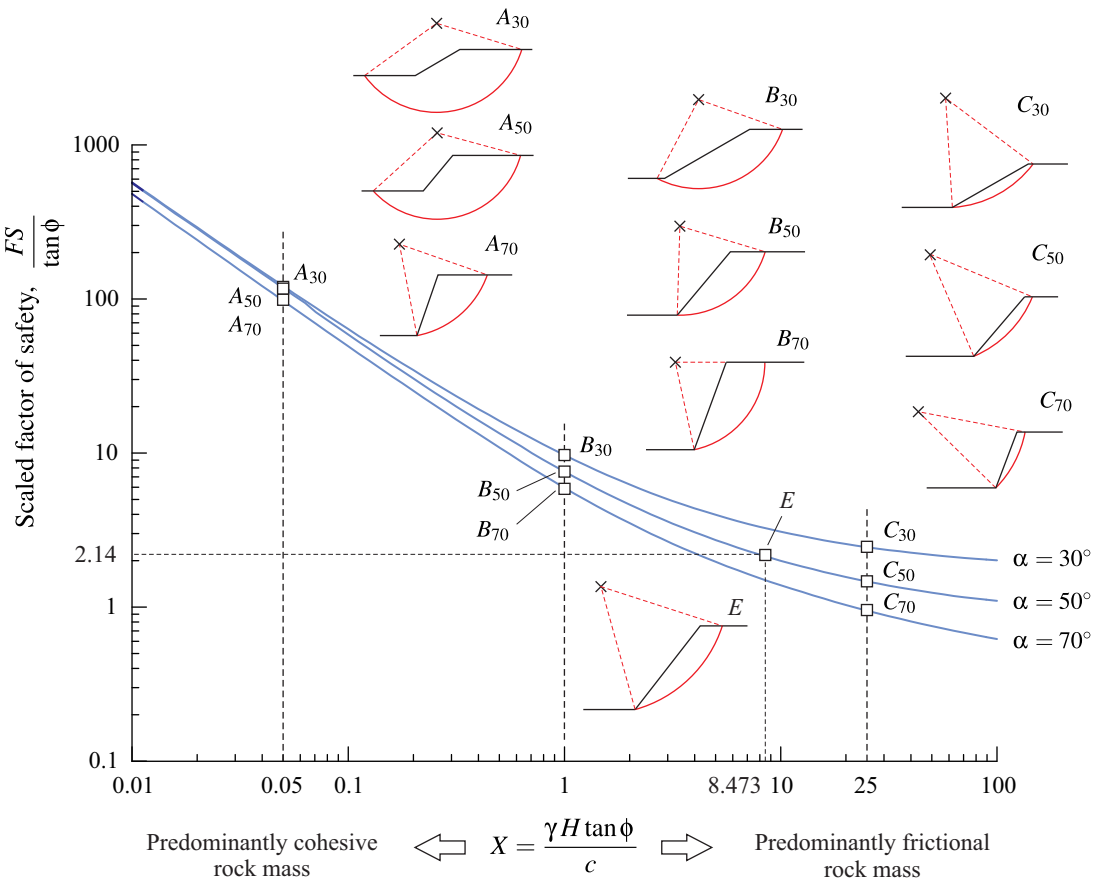

Figure 9. Dimensionless stability diagram showing similarity of scaled factor of safety and critical failure surface location —case of Mohr-Coulomb rock masses.

3.2. Slopes in rock masses that satisfy the Hoek-Brown failure criterion

A similar analysis as presented above for slopes in Mohr-Coulomb rock masses can be done for slopes in rock masses that satisfy the Hoek-Brown failure criterion. The transformation of normal stresses presented in Section 2.2 (equation 10) is applied now to the characteristic measure of normal stress γH used earlier on, to give a dimensionless factor referred to as X [36], i.e.,

$$X = \frac{\gamma H}{m_b \sigma_{ci}} + \frac{s}{m_b^2} \tag{20}$$

For the case of slopes in Hoek-Brown rock masses, the factor of safety and coordinates of points defining the circular failure surface depend also on the dimensionless term s/m_b^2, which will be referred to as the factor Y [36]

$$Y = \frac{s}{m_b^2} \tag{21}$$

Again, from dimensional analysis, considering the transformed version of the Hoek-Brown failure criterion given by equation (11), it can be shown that the factor of safety of the slope in Figure 7 must depend on the factors X and Y above, and on the angle of the slope face, α [36]

$$FS = f_{FS}(X, Y, \alpha) \tag{22}$$

It can also be shown that the scaled coordinates of the points C and A in Figure 7, that define the position of the critical circular failure surface for the slope, depend on the variables X, Y and α only, i.e.,

$$\frac{x_c}{H} = f_{x_c}(X,Y,\alpha); \qquad \frac{y_c}{H} = f_{y_c}(X,Y,\alpha) \tag{23}$$

and

$$\frac{x_A}{H} = f_{x_A}(X,Y,\alpha); \qquad \frac{y_A}{H} = 0 \tag{24}$$

As for the case of slopes in Mohr-Coulomb material, the same equation (12) can be used with equations (23) and (24) to define the radius of the critical failure surface in Figure 7.

To reconstruct the functions in equations (22) through (24), and as done for the case of slopes in Mohr-Coulomb rock masses, the Bishop's method of slices implemented in the limit equilibrium software SLIDE [32] was employed [36]. A total of 60,984 cases of slopes were set up and computed. The input variables in the models were chosen so to obtain 121 equally spaced (in logarithm base-10 scale) slope cases with the factor X ranging between 10^{-4} and 100. Cases were chosen to obtain a total of 14 values of the factor Y, with a minimum value of zero, followed by values of 1×10^{-5}, 2.5×10^{-5}, 5.0×10^{-5}, 1×10^{-4}, etc. up to a maximum value of 0.1. The ranges of values for X and Y were selected by means a Monte-Carlo simulation that yielded the expected ranges of factors X and Y for typical ranges of values of slope heights, unit weights and Hoek-Brown parameters encountered in the practice of rock slope engineering. Face inclination angles between 20° and 70°, in increments of 10°, were chosen. More details about the models can be found in [36].

Figures 10 and 11 show the graphical representation of the function f_{FS} in equation (22), as obtained with SLIDE, for values of the dimensionless factor Y equal to 1.0×10^{-2}, 1.0×10^{-3}, 1.0×10^{-4} and 0, respectively. The diagrams define the relationship between the factor of safety FS (vertical axis) and the dimensionless factor X (horizontal axis) for different slope angles α (the various curves in the diagram). In Figures 10 and 11, the small dots on the curves represent the actual limit equilibrium models that were evaluated.

In Figures 10 and 11, large values of the factor X in the horizontal axes correspond to *weak* rock masses, while small values of X correspond to *strong* rock masses. Consequently, the values of factor of safety that are read on the vertical axis decrease as the value of X increases. It is also important to notice that the different sets of curves in Figures 10 and 11 are asymptotic to vertical lines corresponding to values $X = Y$. This means that the factor of safety becomes infinite when $X \leq Y$. This is understood by the fact that in order to have $X \leq Y$, the term $\gamma H/(m_b\,\sigma_{ci})$ in equation (20) must be zero or negative, and for this to occur, the height of the slope must be zero or negative, when all other variables in equation (20) are larger than zero.

Comparing now the diagrams in Figures 10 and 11a, with the diagram in Figure 11b, as the dimensionless factor Y decreases, the rock mass becomes weaker (the Hoek-Brown parameter s acts as a 'cohesion' component in equation 4). In this regard, for the case $Y = 0$ (Figure 11b), the rock mass has zero unconfined compressive strength and therefore the Hoek-Brown failure criterion predicts the lowest shear strength possible (in the Hoek-Brown failure criterion, the *rock mass* unconfined compressive strength, σ_{cm}, can be obtained by making $\sigma_3 = 0$ in equation (4); therefore, if $s = 0$, then $\sigma_{cm} = 0$). Because of this, the diagram in Figure 11b (for $Y = 0$) can used to obtain a *conservative* measure of factor of safety of slopes in Hoek-Brown rock masses, corresponding to the case in which rock masses do not have unconfined compressive strength. As an example, Point E in Figure 10b represents a slope of inclination angle $\alpha = 50°$ for which $X = 0.1$ and $Y = 1\times10^{-3}$. The diagram predicts a factor of safety $FS = 2.01$. If the same slope is considered in a Hoek-Brown rock mass with $Y = 0$ (i.e., $s = 0$), point E' in Figure 11b now predicts a lower factor of safety $FS = 1.88$.

For space reasons, only diagrams corresponding to dimensionless factors Y equal to 1.0×10^{-2}, 1.0×10^{-3}, 1.0×10^{-4} and 0 are presented in here. Similar diagrams corresponding to other Y values (as mentioned previously, 1×10^{-1}, 5.0×10^{-2}, 2.5×10^{-2}, 1.0×10^{-2}, 5.0×10^{-3}, ... 1.0×10^{-5} and 0) can be found in [36].

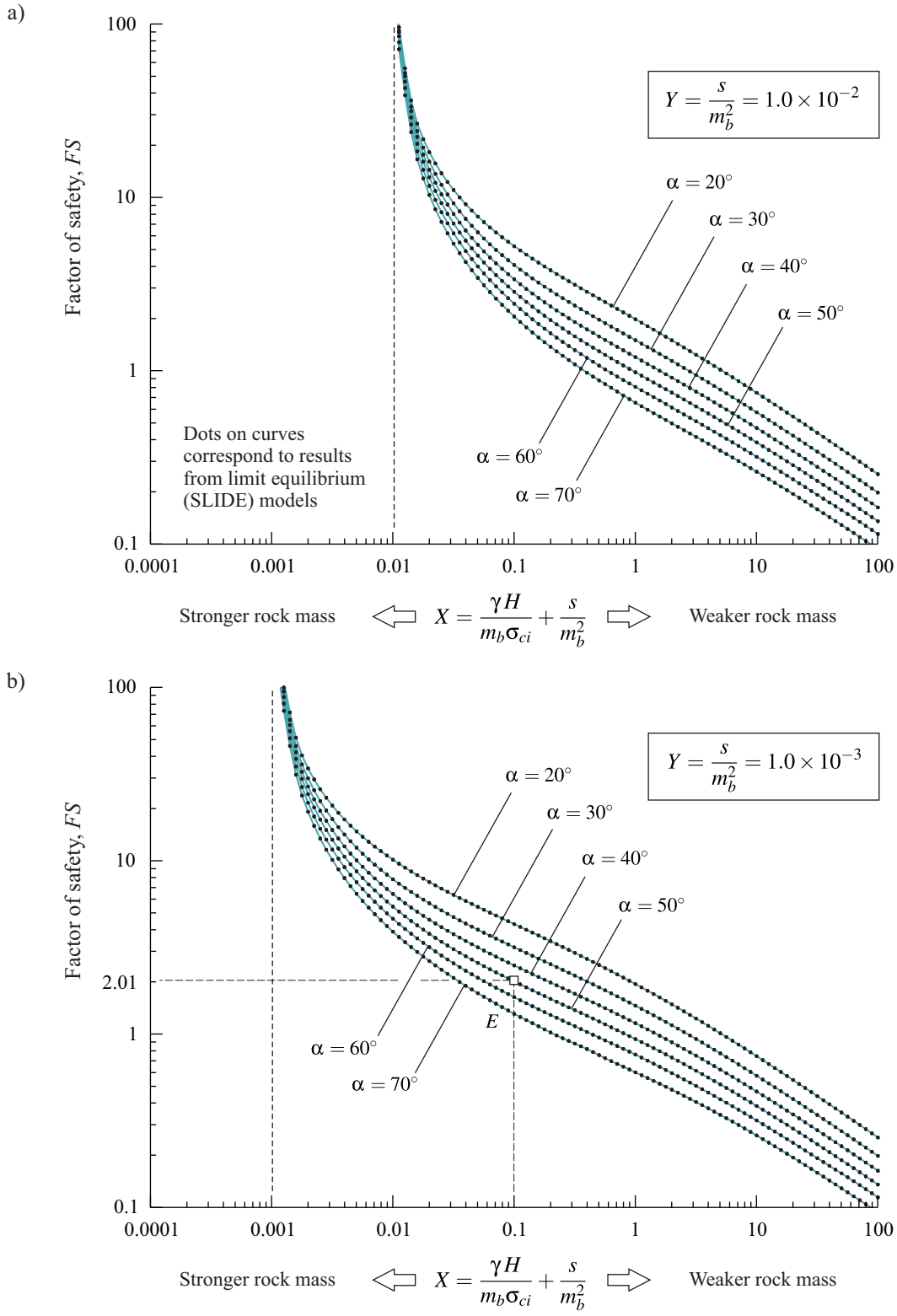

Figure 10. Dimensionless stability diagrams for estimation of factor of safety of slopes in rock masses that satisfy the Hoek-Brown failure criterion. Diagrams correspond to Y factors equal to a) 1.0×10^{-2} and b) 1.0×10^{-3}, respectively.

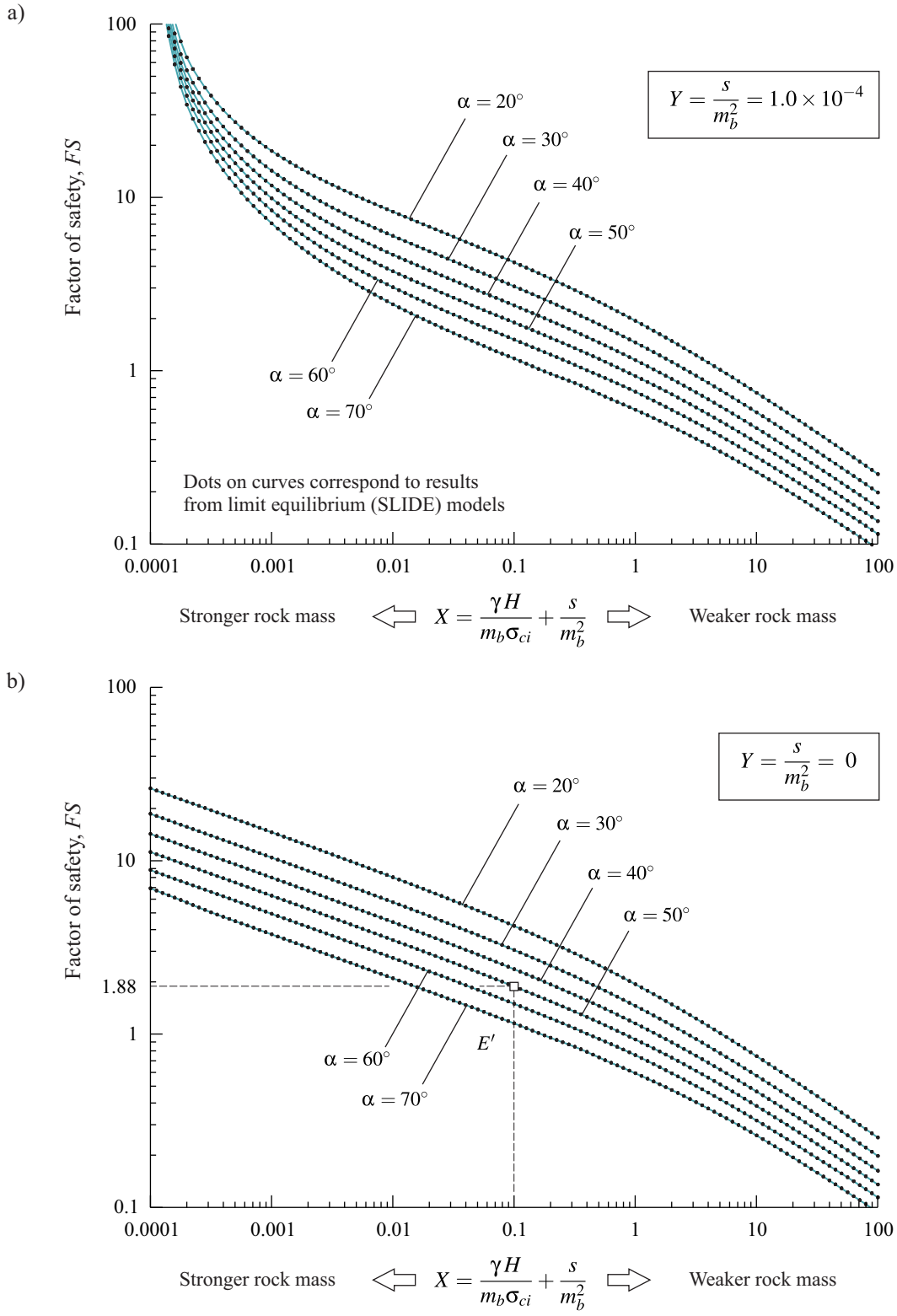

Figure 11. Stability diagrams as in Figure 10 for Y factors equal to a) 1.0×10^{-4} and b) 0, respectively.

Also, for space reasons, no diagrams for the functions f_{x_c}, f_{y_c}, f_{x_A}, and f_{y_A} in equations (23) and (24) are presented in this paper. As for the case of slopes in Mohr-Coulomb rock masses, the diagrams can be constructed using the EXCEL spreadsheet corresponding to slopes in Hoek-Brown rock masses, available for downloading using the links provided in Section 6. For example, for the same point E indicated in Figure 10b, the EXCEL spreadsheet allows to compute the scaled coordinates of the center of the circular failure surface to be $x_c/H = -0.58$ and $y_c/H = 1.63$, and the scaled coordinates of the starting point of the failure surface to be $x_A/H = y_A/H = 0$, this resulting in a scaled radius of the critical failure surface $R/H = 1.73$ —see Figure 7.

Another useful computational tool for slopes in Hoek-Brown rock masses consist of closed-form equations for estimating factors of safety obtained from regression analysis of the functions corresponding to $Y = 0$ in Figure 11b. The equation for computing factor safety obtained from regression analysis is

$$FS(X,\alpha) = 10^{f_0(\alpha)+f_1(\alpha)\log(X)+f_2(\alpha)\log(X)^2+f_3(\alpha)\log(X)^3+f_4(\alpha)\log(X)^4} \tag{25}$$

where the functions f_0, f_1, f_2, f_3 and f_4 are computed as follows:

If $\alpha \leq 50^\circ$

$$\begin{aligned}
f_0(\alpha) &= -3.561\times10^{-2} - 9.200\times10^{-3}(\alpha-50) - 2.489\times10^{-5}(\alpha-50)^2 - 2.439\times10^{-6}(\alpha-50)^3 \\
f_1(\alpha) &= -3.399\times10^{-1} + 8.766\times10^{-4}(\alpha-50) + 2.611\times10^{-6}(\alpha-50)^2 + 3.440\times10^{-7}(\alpha-50)^3 \\
f_2(\alpha) &= -3.288\times10^{-2} + 3.130\times10^{-5}(\alpha-50) - 3.130\times10^{-6}(\alpha-50)^2 - 5.646\times10^{-8}(\alpha-50)^3 \\
f_3(\alpha) &= -3.837\times10^{-3} - 7.899\times10^{-5}(\alpha-50) - 1.126\times10^{-6}(\alpha-50)^2 - 5.010\times10^{-8}(\alpha-50)^3 \\
f_4(\alpha) &= 4.268\times10^{-5} - 1.383\times10^{-5}(\alpha-50) - 1.307\times10^{-7}(\alpha-50)^2 - 7.198\times10^{-9}(\alpha-50)^3
\end{aligned} \tag{26}$$

If $\alpha \geq 50^\circ$

$$\begin{aligned}
f_0(\alpha) &= -3.561\times10^{-2} - 9.092\times10^{-3}(\alpha-50) - 2.465\times10^{-6}(\alpha-50)^2 - 1.280\times10^{-6}(\alpha-50)^3 \\
f_1(\alpha) &= -3.399\times10^{-1} + 7.524\times10^{-4}(\alpha-50) - 3.361\times10^{-6}(\alpha-50)^2 + 9.897\times10^{-7}(\alpha-50)^3 \\
f_2(\alpha) &= -3.288\times10^{-2} + 9.853\times10^{-5}(\alpha-50) + 2.177\times10^{-6}(\alpha-50)^2 - 1.980\times10^{-7}(\alpha-50)^3 \\
f_3(\alpha) &= -3.837\times10^{-3} - 2.470\times10^{-5}(\alpha-50) + 2.392\times10^{-6}(\alpha-50)^2 - 2.413\times10^{-7}(\alpha-50)^3 \\
f_4(\alpha) &= 4.268\times10^{-5} - 5.531\times10^{-6}(\alpha-50) + 4.533\times10^{-7}(\alpha-50)^2 - 3.182\times10^{-8}(\alpha-50)^3
\end{aligned} \tag{27}$$

Equations (25) through (27) allow to reconstruct the different curves in the dimensionless diagram for $Y = 0$ in Figure 11b, and therefore to estimate factors of safety of slopes for the conservative assumption discussed earlier on. The interested reader is referred to [36] for more details about the equations (25) through (27), including an example of application of the equations, and a discussion on the expected differences in values of factor of safety obtained with the equations and with the EXCEL spreadsheet.

The concept of mechanical similarity of slopes introduced in Section 3.1 also applies to slopes in rock masses that satisfy the Hoek-Brown failure criterion. This will be discussed next, again, by means of an example.

Five different cases of slopes excavated in Hoek-Brown rock masses, as listed in Table 6a, are considered. Although the values of slope angle (α) listed in the table are the same for all cases, the values of height (H), unit weight (γ), geological strength index (GSI), disturbance factor (D), unconfined compressive strength (σ_{ci}) and Hoek-Brown parameter (m_i) are different. Consequently, the values of the Hoek-Brown parameters m_b and s listed in the last two columns of Table 6a, which are computed with equations (5) and (6), respectively, are also different (the value of the Hoek-Brown parameter a is considered to be equal to 0.5, as discussed already in Section 2.2).

At first sight, and disregarding the fact that all five cases have the same slope angle ($\alpha = 50^\circ$), these correspond to quite different slopes excavated in Hoek-Brown rock masses.

Table 6. Example of slopes displaying similarity of factor of safety and critical failure surface location —case of Hoek-Brown rock masses.

a)

Case	α [°]	H [m]	γ [kN/m^3]	GSI [-]	σ_{ci} [MPa]	m_i [-]	m_b [-]	s [-]
1		241	27	59	20.4	14	3.24	1.05E-2
2		520	25	77	15.0	20	8.80	7.76E-2
3	50	360	27	42	77.7	10	1.26	1.59E-3
4		676	24	86	11.3	24	14.56	2.11E-1
5		399	26	24	225	7	0.46	2.15E-4

b)

Case	X [-]	Y [-]	FS	x_c/H [-]	y_c/H [-]	x_A/H [-]	y_A/H [-]	R/H [-]
1								
2								
3	0.1	1E-3	2.01	-0.58	1.63	0.00	0.00	1.73
4								
5								

Considering now the first three columns in Table 6b, all five cases are characterized by the same dimensionless factors $X = 0.1$ and $Y = 1 \times 10^{-3}$, given by equations (20) and (21), respectively. Therefore, according to equations (22) through (24), all five slope cases are expected to have the very same values of factor of safety and scaled coordinates of points that define the critical failure surface. Indeed, application of equations (22) through (24), using the EXCEL spreadsheet mentioned earlier on, yields the values of factor of safety and scaled coordinates of points C and A in Figure 7, and the resulting scaled radius of the critical circular failure surface, listed in the remaining columns of Table 6b.

The fact that different combinations of input variables in the slope problem in Figure 7 yield the very same values of dimensionless factors X and Y, and therefore the same values of factor of safety and scaled position of the critical failure surface, implies that mechanical similarity of slopes in Hoek-Brown rock masses is controlled by the dimensionless factors X and Y, and the slope angle α. For this reason, in the reminder of this paper, the dimensionless factors X and Y, defined by equations (20) and (21), will be referred to as the similarity factors X and Y.

The concept of mechanical similarity is further illustrated in Figures 12 and 13. These diagrams are equivalent to those in Figures 10 and 11, respectively. For clarity, curves corresponding to slope angles equal to 30°, 50° and 70° only are included. The different sketches above the curves in Figures 12 and 13 correspond to slope cases in *strong* rock masses (characterized by an arbitrarily chosen value $X = 0.001$ —see points A indicated the diagrams); in *average* rock masses (value $X = 0.1$ —points B in the diagrams), and in *weak* rock masses (value $X = 10$ —points C in the diagrams). The sketches show the position of the critical circular failure surface as obtained with the EXCEL spreadsheet, for each of the six points in the diagrams in Figure 12, and for each of the nine points in the diagrams in Figure 13. The sketches show that the failure surface tends to be deeper for smaller values of slope inclination angles and also deeper for weaker rock masses.

Finally, it should be noted that all five cases listed in Table 6 plot as points B_{50} in Figure 12b. Therefore, the sketch corresponding to case B_{50} in Figure 12b is representative of the shape of the critical circular failure surface for all five cases listed in Table 6.

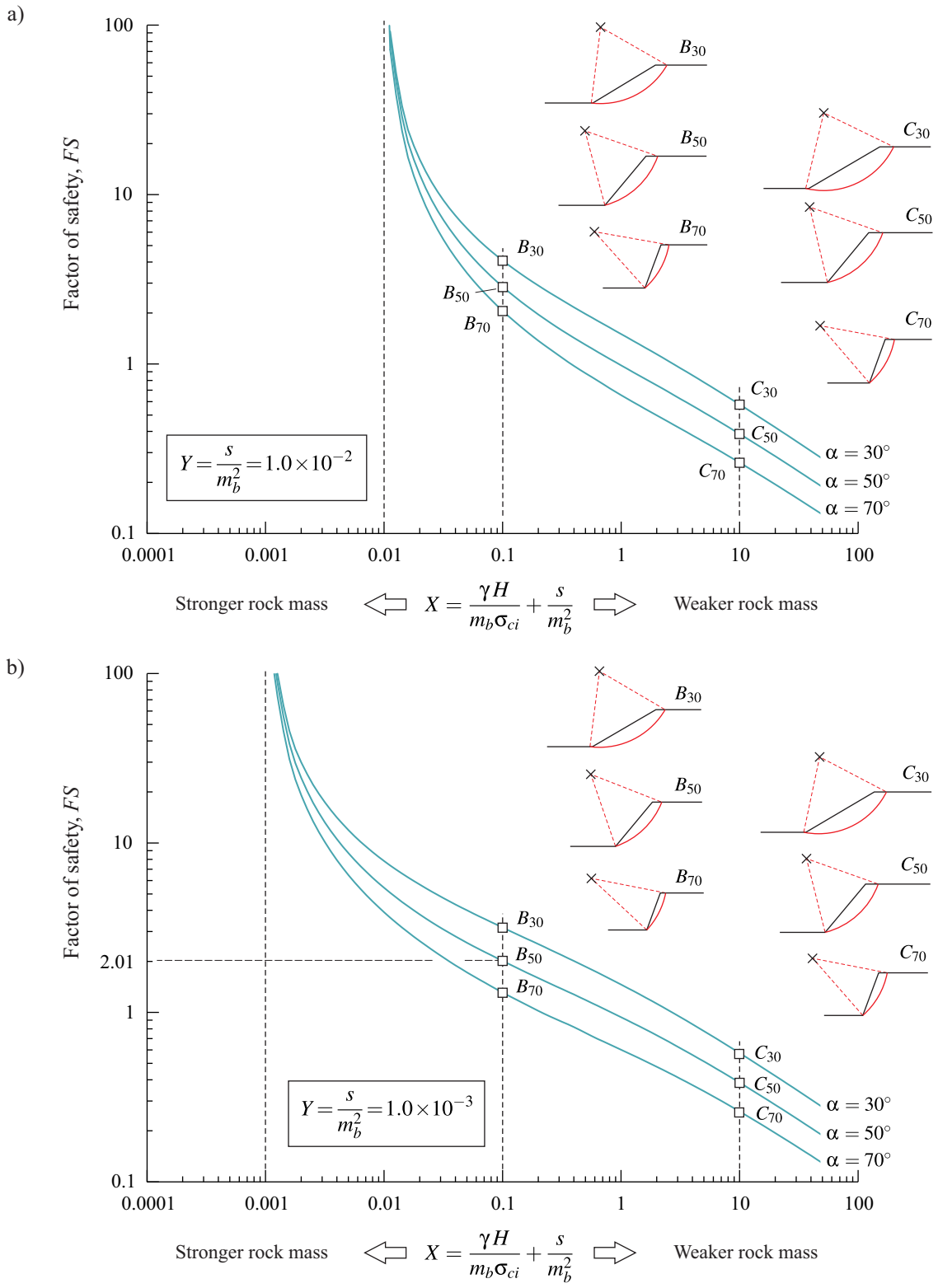

Figure 12. Dimensionless stability diagrams showing similarity of factor of safety and critical failure surface location —case of Hoek-Brown rock masses. Diagrams correspond to Y factors equal to a) 1.0×10^{-2} and b) 1.0×10^{-3}, respectively.

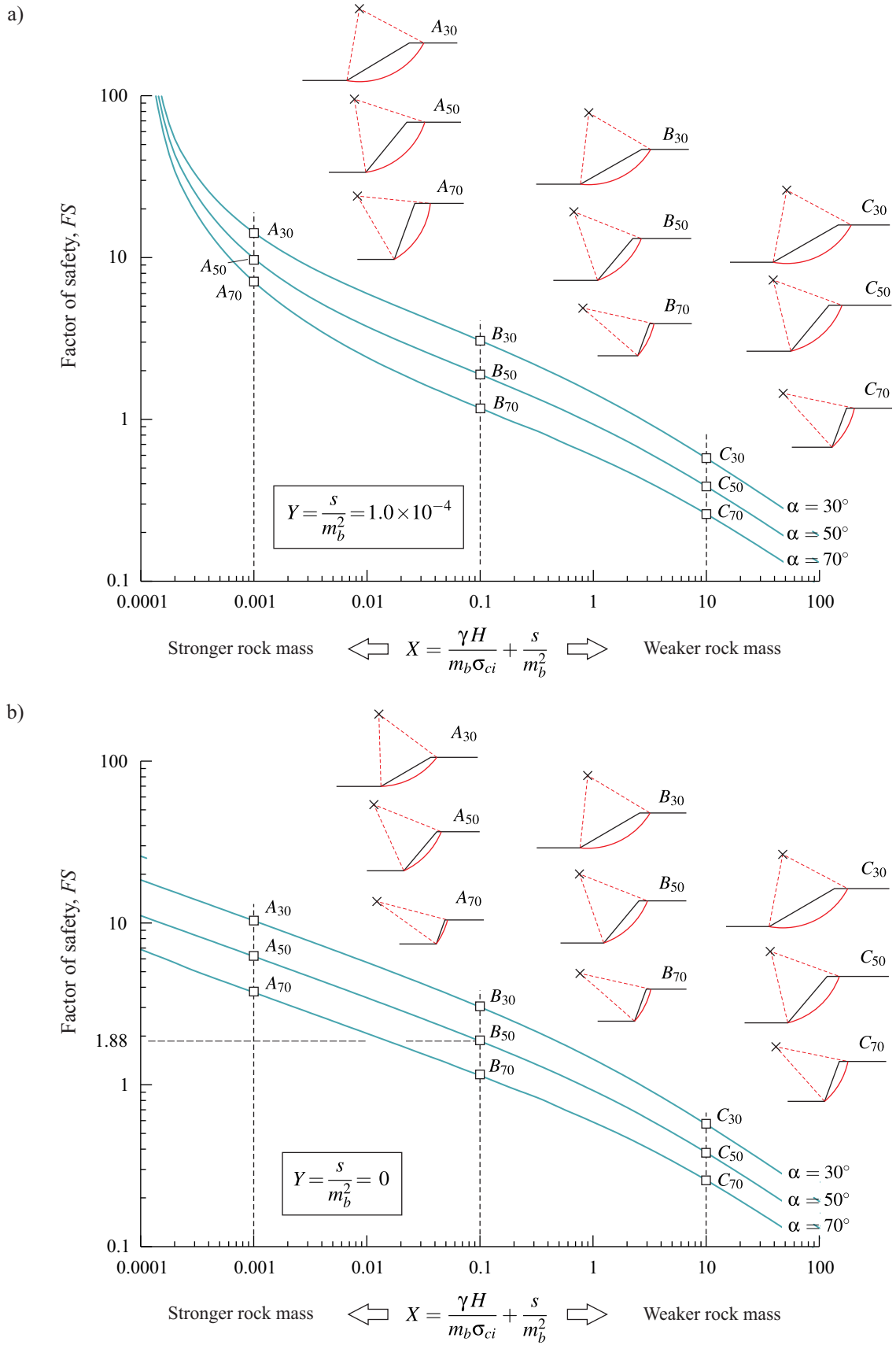

Figure 13. Stability diagrams as in Figure 12 for Y factors equal to a) 1.0×10^{-4} and b) 0, respectively.

4. Application examples

This section presents examples of slope problems analyzed with the computational tools introduced in Section 3. Since the computational tools were developed based on limit equilibrium models, in particular using the software SLIDE [32], the examples also include comparisons of results obtained with the shear strength reduction technique implemented in the software FLAC [33]. The comparison is included to show that stability results obtained with the two methods of analysis are comparable.

4.1. Stability of rock slope in open pit mine

This example involves the analysis of stability of a rock slope in an open pit mine in Chile [36]. A photograph of the rock slope and the list of input variables considered for the problem are shown in Figure 14. The pit slope has 12 benches with a bench height of 30 m and a bench width of 16 m. The bench face angle is 71°. This results in a total slope height, $H = 360$ m, and an overall slope angle measured from toe to crest, $\alpha = 50°$. In this case, and as discussed in the introduction Section 1, the joint spacing is small enough relative to the total slope height, that the Hoek-Brown failure criterion can be applied. The properties of the rock mass are summarized on the right side of Figure 14. Based on these properties, and as indicated also in Figure 14, the similarity factors introduced in Section 3.2 result to be $X = 0.1$ and $Y = 1 \times 10^{-3}$. Therefore, this slope case is also represented by the points E and B_{50} in Figures 10b and 12b, respectively. The values of factor of safety and the coordinates of the center and radius of the critical failure surface in Figure 7, as obtained with the EXCEL spreadsheet in [36], are summarized in Table 7. In particular, the factor of safety results to be 2.01 (i.e., larger than one) so the rock slope is considered stable.

To confirm the validity of the results listed in Table 7, the rock slope in Figure 14 is solved with the software SLIDE, in one instance considering the slope face with the actual benches, and in the other instance considering a planar face linking the toe and crest of the slope. Figure 15a shows the results obtained with the software SLIDE for the first case in which benches are considered. The figure includes the different circular failure surfaces analyzed with the software, using the same search procedure as when developing the computational tools discussed in this paper. Figure 15a shows the critical circular failure surface corresponding to the minimum factor of safety for the slope (this is indicated with a continuum red line in the figure). The factor of safety obtained with the software for the case of slope

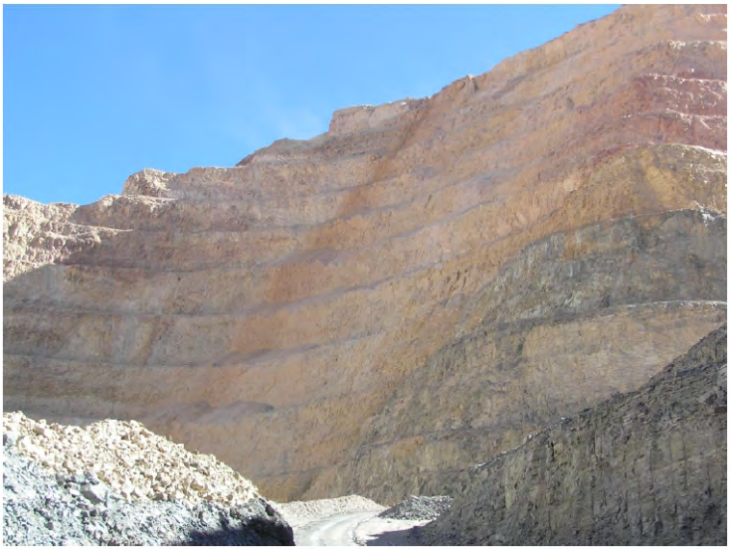

Input data:

$H = 360$ m (slope height)
$\alpha = 50°$ (overall slope angle)

$\gamma = 27$ kN/m^3
$\sigma_{ci} = 77.7$ MPa
$m_i = 10$
GSI $= 42$
D $= 0$
$m_b = 1.2601$
$s = 1.59 \times 10^{-3}$
$a = 0.5$ (assumed)

Dimensionless factors:

$$X = \frac{\gamma H}{m_b \sigma_{ci}} + \frac{s}{m_b^2} = 0.1$$

$$Y = \frac{s}{m_b^2} = 1.0 \times 10^{-3}$$

Figure 14. Application example of stability analysis of rock slope in an open pit mine —after [36].

Table 7. Factor of safety and location of the critical circular failure surface for the slope problem in Figure 14 obtained with EXCEL spreadsheet in [36].

From EXCEL spreadsheet:
– Factor of safety, $FS = 2.01$
– Abscissa of the center of the critical circular failure surface, x_c = -207 m
– Ordinate of the center of the critical circular failure surface, $y_c = 587$ m
– Radius of the critical circular failure surface, $R = 622$ m

with benches is 2.05. Figure 15a also shows the location of the critical failure surface obtained with the software SLIDE and with the EXCEL spreadsheet discussed in Section 3.2, assuming the slope face to be planar (this is indicated with a dashed red line in Figure 15a). For this case, the factor of safety computed with both SLIDE and the EXCEL spreadsheet is 2.01 (see Table 7), this being basically the same value as the one obtained when benches are considered for the rock slope in Figure 15a.

Figure 15b shows the same slope, this time solved with the shear strength reduction technique in the software FLAC —for space reasons, only the case of planar slope face is included here. The factor of safety obtained with FLAC is 2.02, which is similar to the value obtained with the EXCEL spreadsheet (for the slope with a planar face). The location of the critical failure surface obtained with FLAC is highlighted by the contour plot representation in Figure 15b, that shows the distribution of scaled maximum shear strain rate (as mentioned in Section 1, when discussing Figure 15b, 'shear strain' refers to the square root of the second invariant of the deviatoric strain rate, while 'scaled' refers to the shear strain rates having been divided by the maximum value of shear strain rate in the model at that stage). This contour representation corresponds to the model that is about to fail (i.e., at the verge of equilibrium). The location of the circular failure surface obtained with the EXCEL spreadsheet is superimposed on the contour representation, indicating that the critical failure surface obtained with both approaches is also comparable.

4.2. Slope in very weak rock mass

This example is included in the documentation of the software FLAC3D [54] and involves a section of slope in a rock mass that satisfies the Hoek-Brown failure criterion —see Figure 16. The problem was originally presented in [55], in the context of illustrating the application of the shear strength reduction technique for the Hoek-Brown material model in the software RS2 [56].

The rock mass properties considered for this example are listed on the lower right corner of Figure 16. Although [55] did not report the values of geological strength index (GSI) to which this rock mass corresponds, application of equations (5) through (7), using the properties listed in Figure 16, allows to back calculate the GSI value and show that this rock mass corresponds to a very weak one, with a geological strength index GSI = 5 (and D = 0 and $m_i = 1.99$). Considering the value of GSI equal to 5, the quality of this rock mass is so low that it behaves basically as a soil.

To illustrate the point, Figure 17a represents various shear failure envelopes plotted in terms of minor and major principal stresses, which are considered representative of the slope problem in this example. In particular, the curve labelled as 'Hoek-Brown failure envelope ($a = 0.619$)' in Figure 17a is the failure envelope corresponding to the given rock mass properties in Figure 16. In Figure 17a, the minor principal stresses in the horizontal axis are considered to be in the interval 0 to 0.12 MPa, with the upper limit being approximately equal to the unit weight of the rock mass multiplied by half the height of the slope in Figure 16. This interval of stresses is assumed to be representative of the values of mean stresses developing on the failure surface when the slope fails. Figure 17a also shows the best fit Mohr-Coulomb failure envelope to the mentioned Hoek-Brown failure envelope, computed with the equations presented in [38] —and as implemented in the software ROCDATA [46]. The resulting values of Mohr-Coulomb

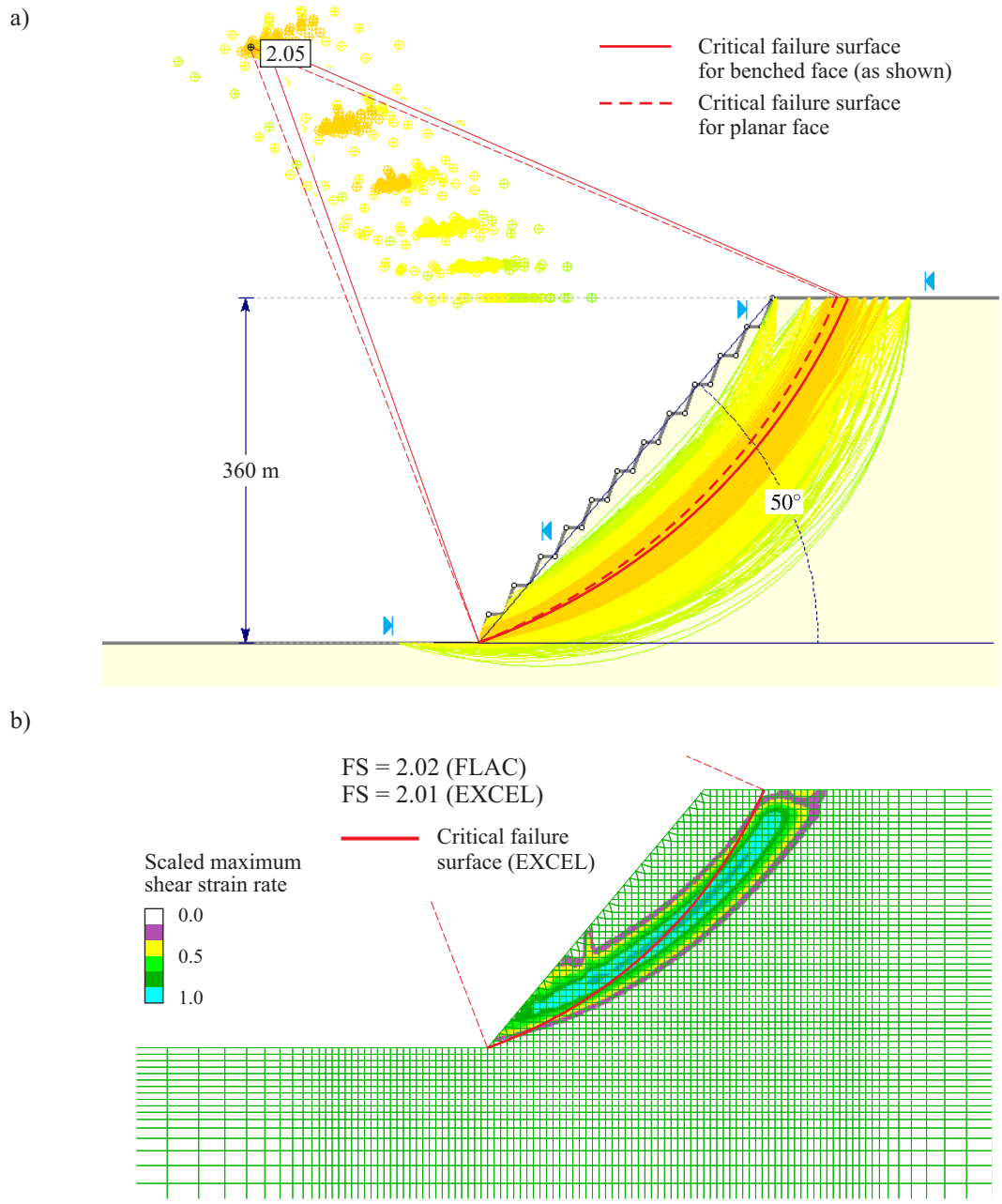

Figure 15. Factors of safety and critical failure surfaces for the slope problem in Figure 14, computed with the software a) SLIDE [32] and b) FLAC [33].

internal friction angle $\phi = 23°$, and cohesion $c = 16.86$ kPa, suggest that the rock mass in this problem is actually a soil.

Although using the Hoek-Brown failure criterion for analyzing the stability of a slope in a rock mass that is basically a soil may be questionable, there is merit in discussing this particular slope problem. The reason is that the problem puts in evidence the limitation of the transformation of the Hoek-Brown failure criterion presented in Section 3.2, with particular reference to the assumption of the Hoek-Brown parameter $a = 0.5$, when the rock mass in question has been evaluated to have a coefficient $a = 0.619$.

Figure 17a represents the Hoek-Brown failure envelope corresponding to the properties listed in Figure 16 but considering the parameter $a = 0.5$ —see curve labelled 'Hoek-Brown failure envelope

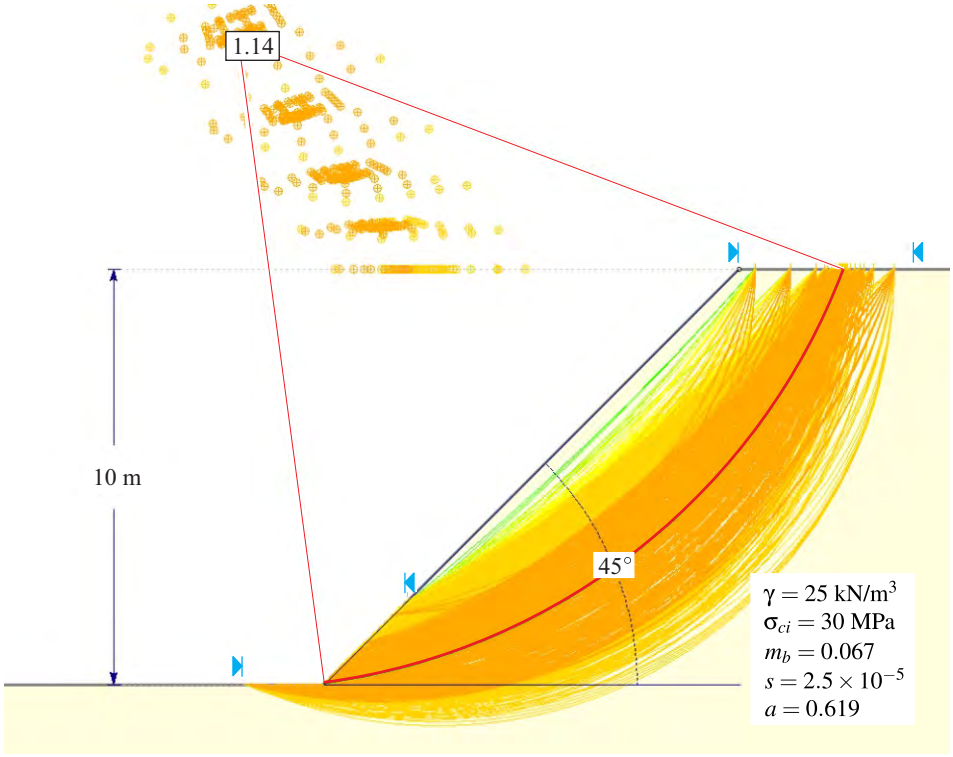

Figure 16. Application example of stability analysis of slope in very weak rock mass —the plot indicates the resulting factor of safety and critical failure surface obtained with the software SLIDE.

($a = 0.5$)'. Clearly the shear strength predicted by the failure envelope that assumes $a = 0.5$ is larger than the one corresponding to the actual coefficient $a = 0.619$ in this example. The diagram in Figure 17b further illustrates this fact. The vertical axis in this diagram represents the ratio of the major principal stress computed with equation (4), assuming $a = 0.5$, and the major principal stress computed with the same equation, but considering the value of the parameter a given by equation (7). The ratio quantifies the over-prediction of shear strength as a function of the geological strength index (GSI). The different curves in Figure 17b suggests that the over-prediction of shear strength starts to become significant for values of GSI smaller than approximately 40. For a value GSI = 5, as in the slope problem considered here, the over-prediction of strength is above 200% for the interval of minor principal stresses between 0 and 0.12 MPa.

Table 8 lists the values of factor of safety and coordinates of points defining the critical failure surface for the slope problem in Figure 16, obtained with various methods. For the given Hoek-Brown properties, considering $a = 0.619$, the software SLIDE predicts a factor of safety equal to 1.14. As discussed above, the EXCEL spreadsheet introduced in Section 3.2, that assumes $a = 0.5$, over-predicts the factor of safety, giving a value of factor of safety equal to 2.39. For the equivalent Mohr-Coulomb properties listed in Figure 17a, the EXCEL spreadsheet introduced in Section 3.1 gives a factor of safety equal to 1.13, which is very similar to the one given by SLIDE for the given Hoek-Brown properties (i.e., considering $a = 0.619$).

Table 8 also lists the value of factor of safety obtained with the shear strength reduction technique in the software FLAC, which results equal to 1.12 (again, a value similar to that predicted with SLIDE and with the EXCEL spreadsheet for equivalent Mohr-Coulomb properties).

Finally, Figure 18 represents the contours of scaled maximum shear strain rate obtained with the software FLAC —the representation is similar to that discussed in Figure 15b in the previous example.

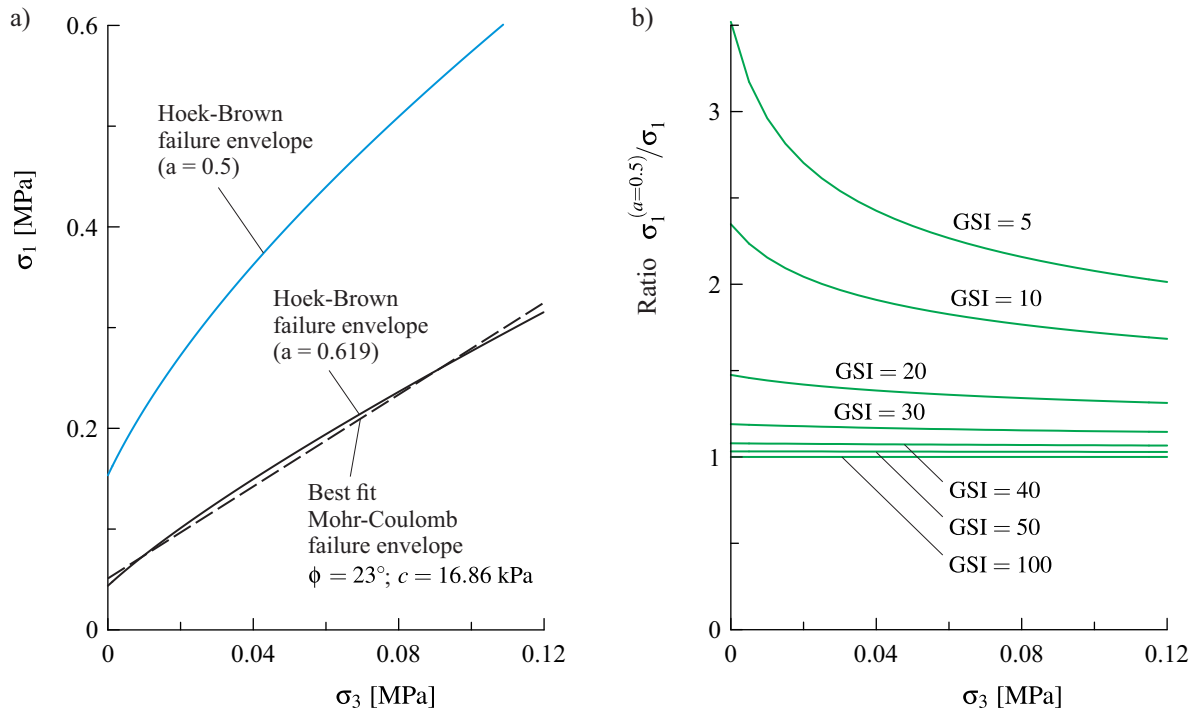

Figure 17. a) Shear strength failure envelopes considered for the rock mass in the problem of Figure 16. b) Overestimation of the major principal stress at failure when assuming that the Hoek-Brown parameter a in equation (4) is 0.5.

Table 8. Factors of safety and locations of critical failure surface for the slope problem in Figure 16 obtained with various methods.

From limit equilibrium model (SLIDE), for given Hoek-Brown properties:
– Factor of safety, $FS = 1.14$
– Abscissa center circular failure surface, $x_c =$ -2.10 m
– Ordinate center circular failure surface, $y_c = 15.52$ m
– Radius circular failure surface, $R = 15.65$ m
From EXCEL spreadsheet in [36], for Hoek-Brown properties, considering $a = 0.5$:
– Factor of safety, $FS = 2.39$
– Abscissa center circular failure surface, $x_c =$ -1.65 m
– Ordinate center circular failure surface, $y_c = 15.26$ m
– Radius circular failure surface, $R = 15.35$ m
From EXCEL spreadsheet in [35], for equivalent Mohr-Coulomb properties:
– Factor of safety, $FS = 1.13$
– Abscissa center circular failure surface, $x_c =$ -1.76 m
– Ordinate center circular failure surface, $y_c = 15.47$ m
– Radius circular failure surface, $R = 15.57$ m
From finite difference model (FLAC), for given Hoek-Brown properties:
– Factor of safety, $FS = 1.12$

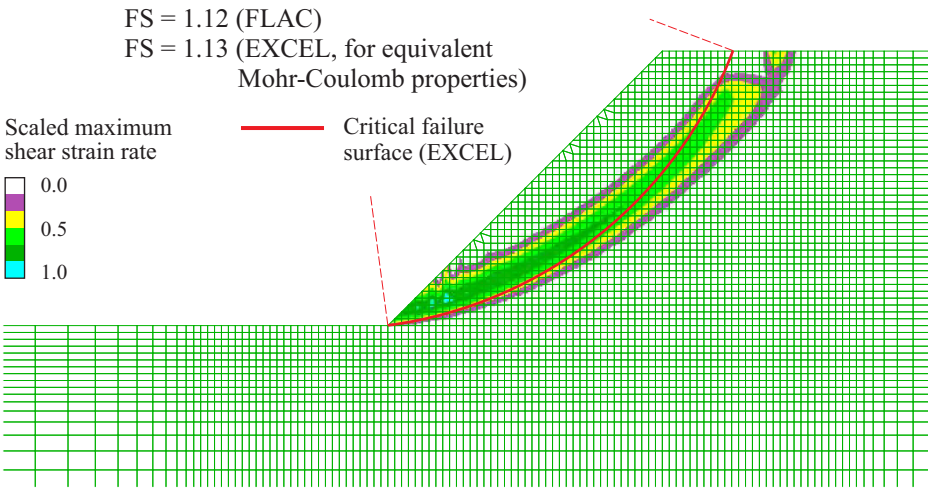

Figure 18. Factors of safety and critical failure surfaces for the slope problem in Figure 16 obtained with FLAC and with the EXCEL spreadsheet in [35].

Figure 18 also includes the outline of the critical failure surface computed with the EXCEL spreadsheet for Mohr-Coulomb material (with the values of equivalent friction and cohesion indicated in Figure 17a), constructed from the coordinates of points listed in Table 8. The location of the critical surface obtained with both methods is similar.

4.3. Rock fill slope versus excavated slope

The example itself and the full background theory for this example are presented in [37]. Although the example considers an embankment made of *soil* that obeys the Mohr-Coulomb failure criterion (i.e., the values of unit weight and Mohr-Coulomb properties used in the example are relatively low for typical waste dumps, stock piles and rock fill dams in mining) the observations derived from this example apply to the case of slopes made of rock fill material too. Because of this, and to avoid confusion, in the reminder of this section the word *embankment* will be used in lieu of the word *rock fill*.

The problem to be analyzed, which is represented in Figure 19, involves an embankment of material that satisfies the Mohr-Coulomb shear strength model, constructed on top of a firm horizontal surface (e.g., a flat rock foundation). The problem consists in determining the factor of safety and location of the critical failure surface under two different scenarios: *i)* when the firm foundation is located at the base of the embankment, as represented in Figure 19a; *ii)* when the firm foundation is located at a great depth, so that the material of embankment and foundation are the same, and the problem becomes that of the same slope introduced in Figure 7. As indicated in Figure 19, the two situations will be referred to as Cases 1 and 2, respectively. For Case 1 (firm foundation below the embankment), the critical failure surface will be assumed not to be able to cut through the firm foundation. The main objective of this example is to discuss which of the two cases leads to the less stable condition —an observation that may not result obvious at first sight.

The bottom part of Figure 19a lists the material properties considered for both the embankment (Case 1) and the slope (Case 2). In particular, it is seen that the combination of input values yields a similarity factor $X = 1$, that according to the horizontal axis in Figures 8 and 9, corresponds to the case of embankment/slope somewhere in the middle of the spectrum of predominantly cohesive and predominantly frictional Mohr-Coulomb material.

For Case 1, similar computational tools (including an EXCEL spreadsheet) as presented for Case 2 in Section 3.1 are provided in [37] —see Section 6. The corresponding computational tools have been

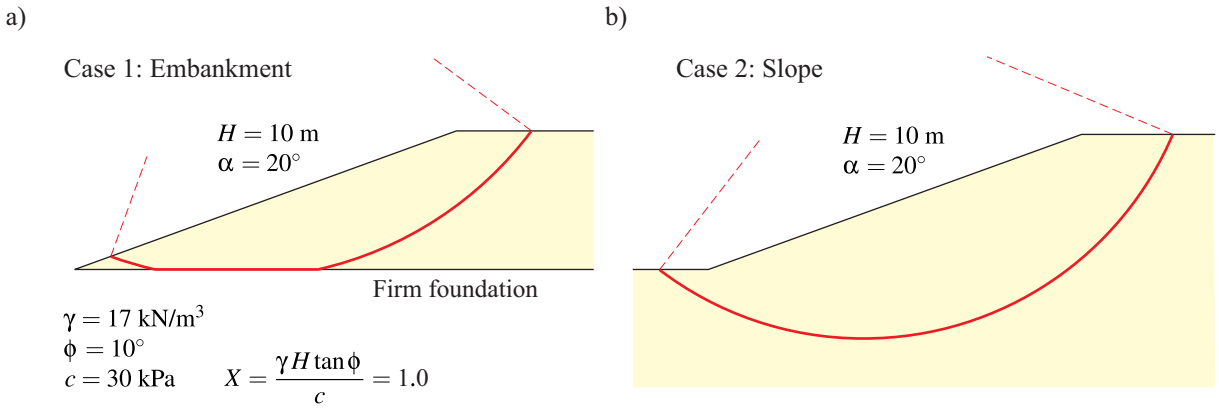

Figure 19. Application example involving assessment of stability conditions for a rock fill (embankment case) and a cut (slope case) in the same material —after [37].

Table 9. Factors of safety and locations of the critical circular failure surfaces for the embankment and slope cases in Figure 19, obtained with EXCEL spreadsheet in [37].

Case 1 (Embankment), from EXCEL spreadsheet:
– Factor of safety, $FS = 2.32$
– Abscissa center circular failure surface, $x_c = 11.7$ m
– Ordinate center circular failure surface, $y_c = 26.0$ m
– Radius circular failure surface, $R = 26.7$ m
Case 2 (Slope), from EXCEL spreadsheet:
– Factor of safety, $FS = 2.02$
– Abscissa center circular failure surface, $x_c = 11.3$ m
– Ordinate center circular failure surface, $y_c = 21.5$ m
– Radius circular failure surface, $R = 26.3$ m

applied to estimate factors of safety and locations of the critical failure surface for Cases 1 and 2 in Figure 19, and the results are summarized in Table 9.

The first observation made from Table 9 is that the factor of safety for Case 1 ($FS = 2.32$) is higher than the one for Case 2 ($FS = 2.02$). As discussed in [37], the dimensionless representations of stability corresponding to each of the cases, show that Case 1 will be more stable than Case 2 provided the inclination angle of the embankment/slope face is less than approximately 50°. This is because for embankment/slope inclination angles larger than this approximate value, the failure surface always starts at the toe of the slope and it does not cut the horizontal plane containing the toe of the slope (i.e., it does not cut any firm foundation that may exist at the base of embankment). The dimensionless representations presented in [37] also show that the difference in the values of factors of safety for both cases depend on the value of the similarity factor X. The smaller the factor X (i.e., the less frictional the material is), the smaller the difference in resulting factors of safety.

Cases 1 and 2 have been also solved with the shear strength reduction technique in the software FLAC. The details of the numerical models are discussed in [37]. Figures 20a and 20b show the resulting contours of scaled maximum shear strain rate for the models corresponding to Cases 1 and 2, respectively (these are similar representations as discussed earlier on, in Figures 15b and 18). The figure also lists

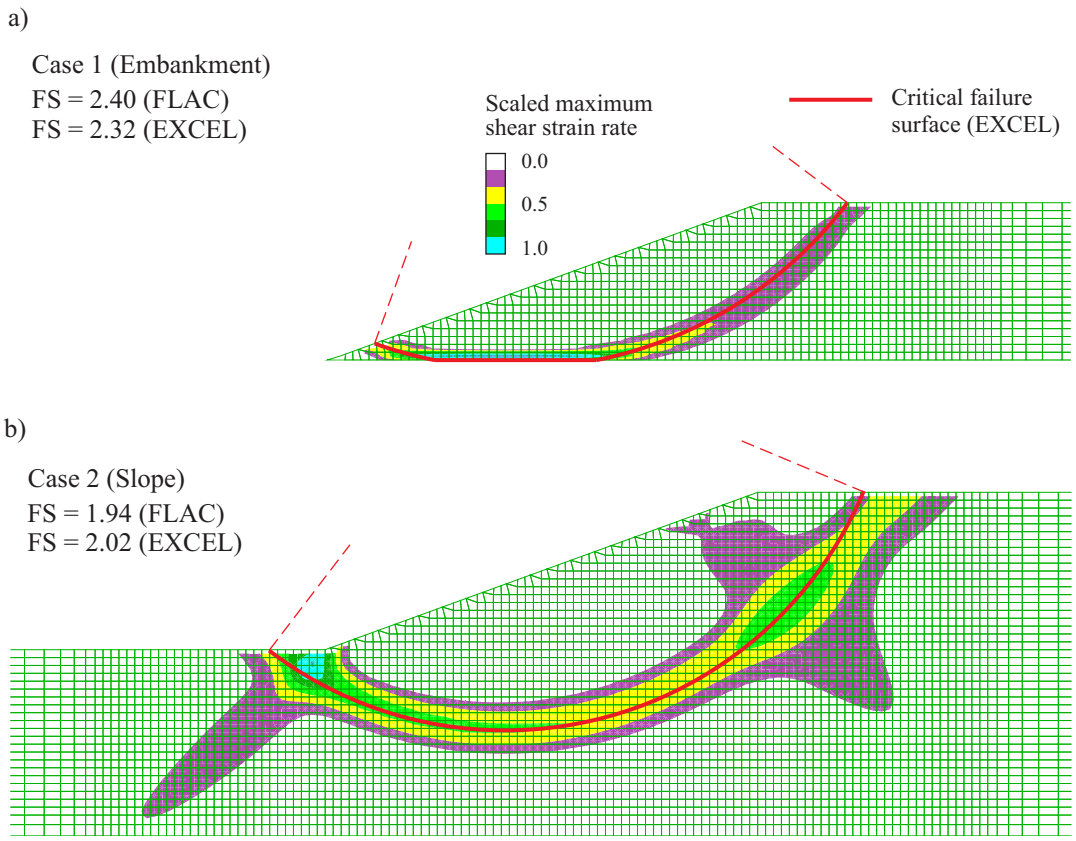

Figure 20. Factors of safety and critical failure surfaces for a) the embankment case, and b) the slope case in Figure 19, obtained with FLAC and with EXCEL spreadsheet in [37].

the values of factor of safety obtained with FLAC for each of the cases; these are generally comparable to the ones obtained with the computational tools, listed in Table 9 —the differences and reasons of the differences are discussed in [37]. The location of the circular failure surfaces obtained with the EXCEL spreadsheets are superimposed on the contour representations in Figure 20, indicating again that the critical failure surface obtained with both approaches is comparable.

4.4. Slopes in dry and water bearing rock masses

This example is also included in the documentation of the software FLAC3D [54] and involves computing factors of safety and locations of critical failure surfaces for slopes in rock masses that satisfy the Mohr-Coulomb failure criterion. Cases of dry rock masses and water bearing rock masses are considered. The objective of the example is to show the effect of water in the rock mass on the overall stability of the slopes for different hydraulic scenarios.

The original example in the documentation of the software FLAC3D compares the shear strength reduction technique results with those obtained from the dimensionless charts developed by Hoek and Bray [5], mentioned in Section 3.1. For space reasons, the application of those particular charts will not be discussed here.

Figure 21 shows the base case of a slope in dry rock mass. The right side of Figure 21 lists the input variables for the slope problem. The factor of safety and location of critical circular failure surface obtained with the software SLIDE are indicated in the figure.

Figure 22a, 22b and 22c show the same slope with three phreatic level configurations, referred to as

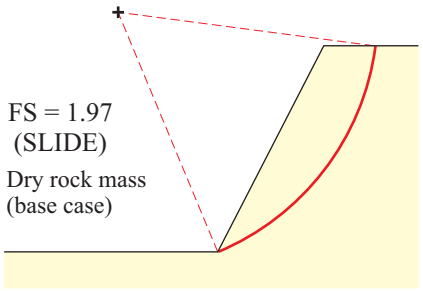

Input data:

$H = 25$ m

$\alpha = 63°$

$\gamma_{dry} = 25$ kN/m^3

$\gamma_{sat} = 26$ kN/m^3

$\gamma_{wat} = 10$ kN/m^3

$\phi = 45°$ (effective)

$c = 100$ kPa (effective)

Resulting dimensionless factors:

$$X = \frac{\gamma H \tan\phi}{c} = 6.25 \quad (\text{for } \gamma = \gamma_{dry})$$
$$= 6.50 \quad (\text{for } \gamma = \gamma_{sat})$$

Figure 21. Application example involving assessment of stability conditions for slopes in dry and water bearing rock masses.

Cases 2, 3 and 4, respectively —these three cases were originally proposed and discussed in [5]. Cases 2 and 3 consider phreatic surfaces defined by a Kozeny's parabola [57] that has the focus at the toe of the slope, and becomes horizontal and coincident with the upper horizontal surface at the crest of the slope, at distances equal to 8 and 4 times the height of the slope —these are the phreatic surface configurations designated as configurations A and B, in Figures 22b and 22c, respectively. Case 4 (Figure 22d) considers the phreatic surface to be coincident with the entire boundary of the slope. This situation corresponds to a slope in a rock mass that is fully saturated.

Figures 22e and 22f show two additional slope cases, to be referred to as cases Cases 5 and 6, respectively, in which the slope is flooded. In the first case the water level is at crest of the slope (Case 5), and in the second case the water level is at a distance of one time the height of the slope above the crest of the slope (Case 6) —these two water level configurations are designated as configurations C and D in Figures 22e and 22f, respectively.

Cases 5 and 6, which were not discussed in [5], are included in this example because the cases are similar to Case 4 (Figure 22d) and these show the mechanical effect of ponding water on the stability of a slope. These cases of flooded slopes may also be of interest for the analysis of stability of underwater slopes in the broader geotechnical engineering field, e.g., in dredging applications.

With regard to the different cases introduced in Figures 21 and 22, it may not be obvious at first sight how to sort the slope cases in order of most stable (i.e., slope with highest resulting factor of safety) to least stable (i.e., slope with lowest resulting factor of safety), or vice-versa, unless any of the computational tools listed in Table 1 is used to evaluate factors of safety for all cases. Indeed, at this point, it is proposed to the reader to carefully look at the Cases 1 through 6 in Figure 22, before continuing reading this section, to try to identify the correct order of most stable to least stable slope configuration.

Table 10 summarizes the resulting factors of safety and scaled coordinates of points that define the critical failure surface for all six cases in Figure 22, as obtained with limit equilibrium models. Table 10 indicates that the correct order of most stable to least stable hydraulic configurations for the slope cases is as follows: Cases 5 and 6 (most stable; $FS/\tan\phi = 2.51$); Case 1 ($FS/\tan\phi = 1.97$); Case 2 ($FS/\tan\phi = 1.88$); Case 3 ($FS/\tan\phi = 1.78$); and Case 4 (least stable; $FS/\tan\phi = 1.10$).

The evaluation of Case 1 can be readily done with the computational tools discussed in Section 3.1. For example, Figure 23 shows a dimensionless diagram similar to that discussed in Figure 9, this time for the slope inclination angle $\alpha = 63°$, considered in this example (see Figure 9). As indicated on the right side of Figure 21, the similarity factor X for the slope in dry rock mass is equal to 6.25, so the point B_1 in the diagram in Figure 23 defines the scaled factor of safety to be $FS/\tan\phi = 1.97$ —also, since the effective internal friction angle is $\phi = 45°$ (see Figure 21), then the actual factor of safety is $FS = 1.97$. The diagram in Figure 23 also includes a sketch of the slope with the location of the critical failure surface, labelled as B_1 —this sketch is similar to the one included in Figure 21. As in the case

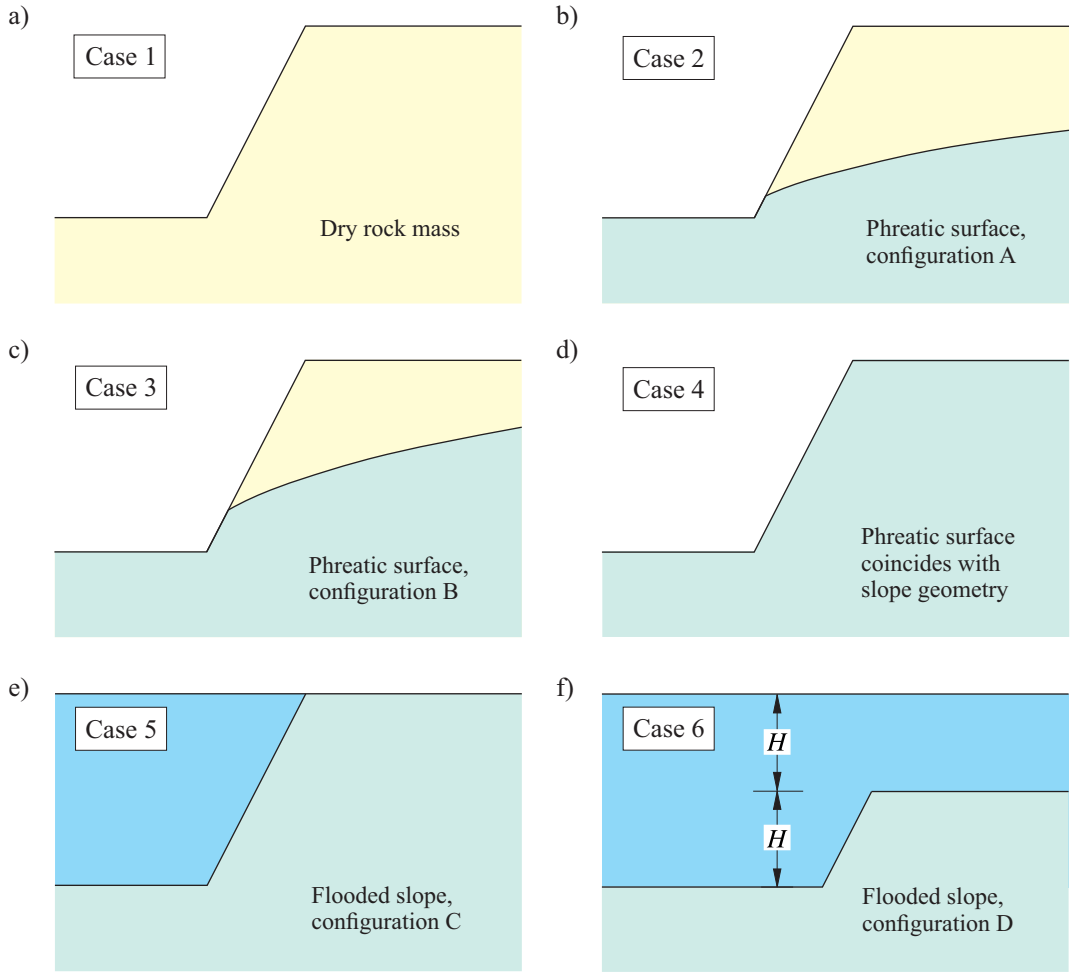

Figure 22. Different hydraulic conditions considered for the slope problem in Figure 21. a) Case of dry rock mass. b) and c) Cases of phreatic surfaces defined by a parabola, with the focus at the toe of the slope, and the phreatic surface intersecting the horizontal surface at the crest of the slope, at distances b) 8 times and c) 4 times the height of the slope, behind the toe. e) and f) Cases of flooded slopes with water levels at e) the crest of the slope, and f) one time the height of the slope above the crest.

Table 10. Factors of safety and locations of the critical circular failure surfaces for the slope cases in Figure 22.

Case	FS [-]	x_c [m]	y_c [m]	R [m]
1*	1.97	-12.43	29.16	31.70
2	1.88	-8.83	25.00	26.51
3	1.78	-8.63	25.00	26.45
4	1.10	-9.62	25.00	26.78
5	2.51	-8.35	26.88	28.14
6	2.51	-8.35	26.88	28.14

* From EXCEL spreadsheet in [35]. Results for all other cases, from limit equilibrium models (SLIDE).

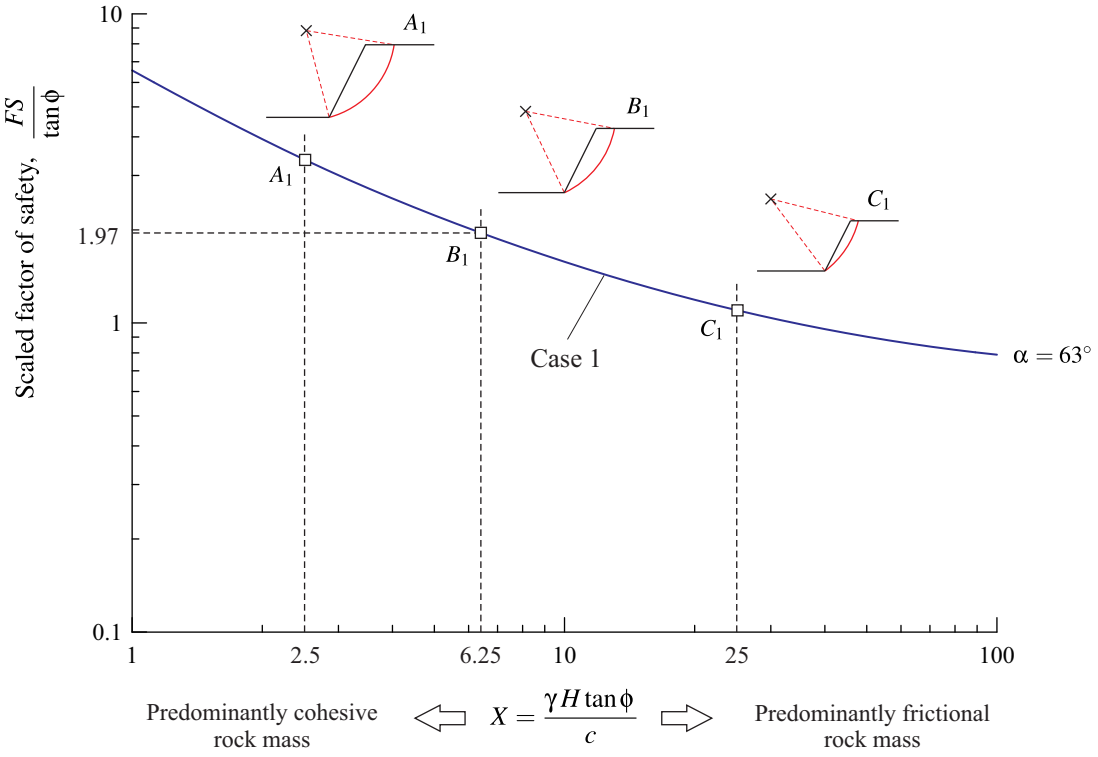

Figure 23. Dimensionless stability diagram for slopes of inclination angle 63° in dry rock mass (Case 1 in Figure 22). The particular slope considered in this example (Figure 21) is represented by point B_1 in the diagram.

of the Figure 9 discussed in Section 3.1, Figure 23 also includes additional points labelled as A_1 and C_1 showing how the factor of safety and the location of the critical failure surface would change if the similarity factor X for this example were to change from one corresponding to a predominantly cohesive rock mass, to one corresponding to a predominantly frictional rock mass.

The software SLIDE has been used to construct similar dimensionless diagrams as in Figure 23, for all remaining slope cases introduced in Figure 22. Figure 24 includes the dimensionless representation of stability for Cases 2, 3 and 4, while Figure 25 includes the dimensionless representation of stability for Cases 5 and 6.

The following observations apply to the results summarized in Table 10 and in Figures 23, 24 and 25.

Cases 5 and 6 are the most stable slope cases and the resulting factor of safety and location of the critical failure surface are the same for both cases. The reason why these two cases yield the highest factor of safety is because although there is water in the rock mass, decreasing the effective normal stresses and so the shear strength on the failure surface (as compared with the case of dry rock mass), the water provides a mechanical pressure on the face of the slope, acting as a buttressing support, and thus increasing the factor of safety of the slope with respect to the base Case 1 (dry rock mass).

The fact that both Cases 5 and 6 are characterized by the same factor of safety is because the effective normal stress along the failure surface, which controls the shear strength of the rock mass and thus the resulting factor of safety for the slope, remains the same for both cases (i.e., both the total normal stress and the water pressure increases when passing from Case 5 to Case 6, but the effective normal stress remains unchanged). It must be emphasized that the factor of safety for Case 5 and Case 6 will be the same independently of the position of the water surface considered in Case 6, provided the water is above the crest of the slope, so the slope is fully flooded.

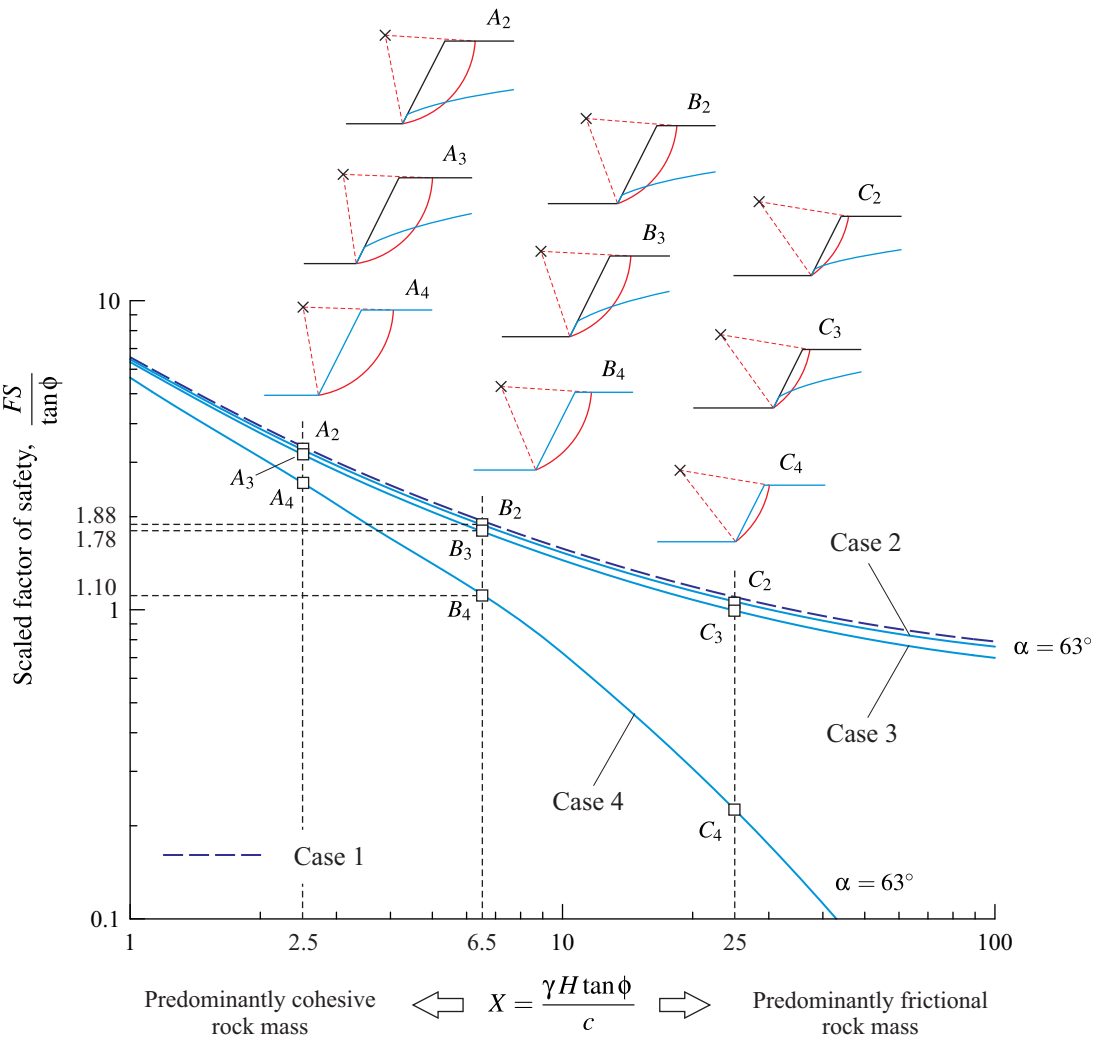

Figure 24. Similar dimensionless representation as in Figure 23 for Cases 2, 3 and 4 in Figure 22. Points B_2, B_3 and B_4 in the diagram represent the particular slopes analyzed in this example.

After Cases 5 and 6, the base Case 1 (dry rock mass) is the most stable case, with Cases 2, 3 and 4 following in decreasing order of stability. The reason why Cases 2, 3 and 4 are less stable than Case 1 is because the water pressure in the ground decreases the normal effective stress on the failure surface, reducing in this way the factor of safety of the slope. Cases 2, 3 and 4 correspond to phreatic surfaces that are closer and closer to the face of the slope, leading in this way to an increasing effect of water in reducing the shear strength of the rock mass on the failure surface. It should be noticed that Case 4 is basically similar to Case 5, except that Case 4 does not have the buttressing effect of the pond water acting on the face of the slope, leading this to a marked reduction of factor of safety for Case 4 with respect to Case 5.

As in previous examples, the cases represented in Figure 22 have also been solved with the shear strength reduction technique implemented in the software FLAC. The stability results for the numerical models corresponding to the different cases in Figure 22 are shown in Figure 26 (the interpretation of the contour representations in the different models in Figure 26 is similar to that discussed for previous examples). The values of factor of safety and the location of the critical failure surface obtained with both methods result generally similar, although the shape of the failure surface given by the shear strength

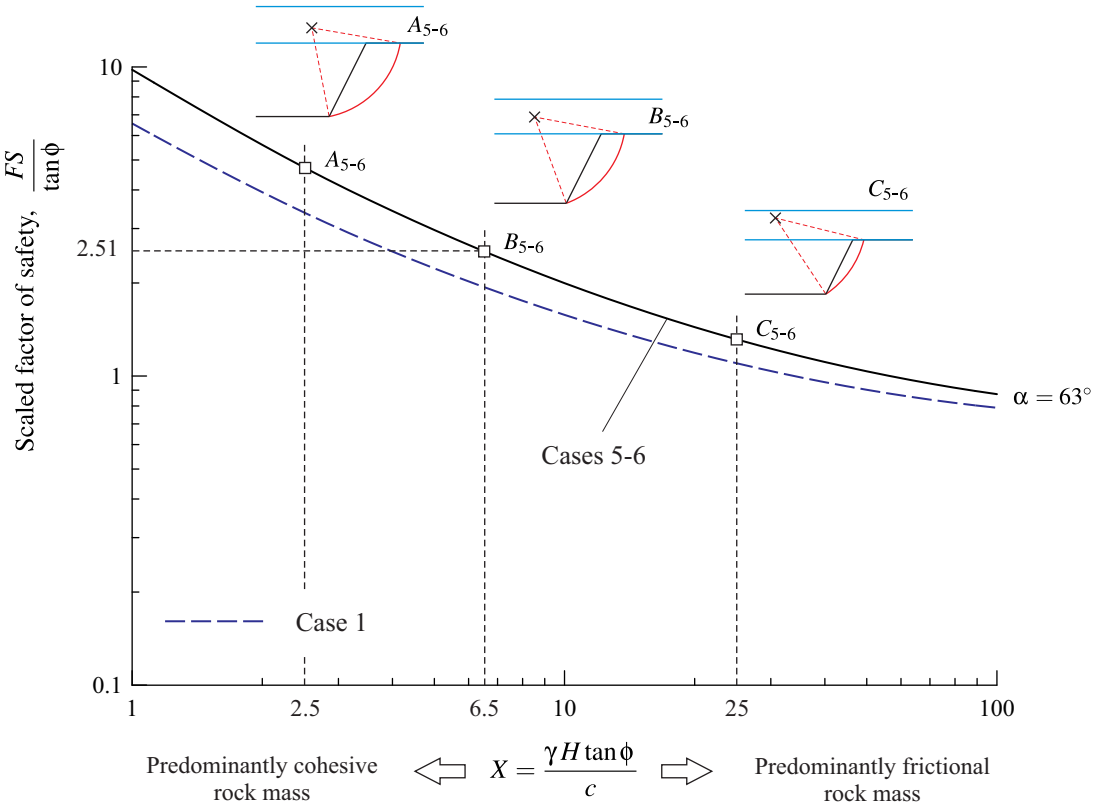

Figure 25. Similar dimensionless representation as in Figures 23 and 24 for Cases 5 and 6 in Figure 22. Point $B_{5\text{-}6}$ in the diagram represents the particular slope analyzed in this example.

reduction technique does not appear to be geometrically circular for most of the cases.

5. Final Comments

The computational tools discussed in this paper, including graphical dimensionless representations, EXCEL spreadsheets, and regression analysis equations, can be used to estimate factors of safety and locations of critical circular failure surfaces for simple rock slopes in homogeneous rock masses or rock fills that satisfy the Mohr-Coulomb or Hoek-Brown failure criteria. Application of this type of tools is useful in the preliminary stages of design of rock slopes in open pit mining, when different slope angles or heights, or different rock mass properties have to be evaluated. The computational tools can also be useful when performing probability and reliability analyses of stability of slopes using simulation approaches like the Monte-Carlo or Bayesian techniques; in these cases, a large number of slope cases and input parameters need to be evaluated —see, for example, [58, 59, 60, 61]. It must be emphasized though that the applicability of the computational tools discussed in this paper is always conditioned by the validity of the assumption of development of a circular (or rotational) failure surface. In the case of slopes in rock masses, this depends on the height of the slope in relation to the degree of jointing and joint spacing in the rock mass —e.g., on the applicability of the Hoek-Brown failure criterion, that assumes the rock mass is homogeneous and isotropic.

The implementation of the transformed versions of the Mohr-Coulomb and the Hoek-Brown failure criteria discussed in Section 2, allowed the number of input variables in the rock slope problem to be reduced and consequently, compact representations of results obtained with limit equilibrium models to be produced. Not having used the transformed versions of these criteria would have required the need of

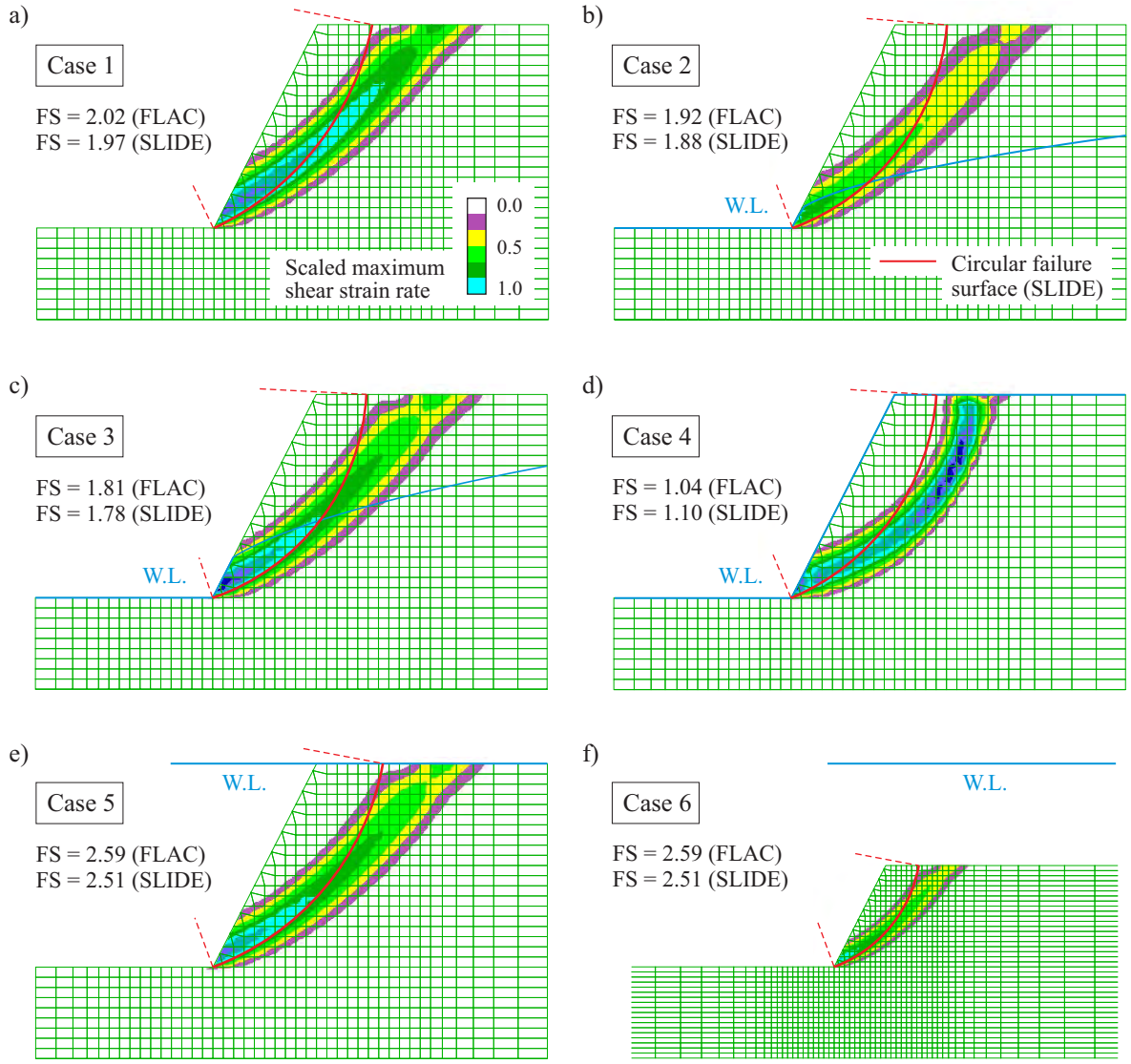

Figure 26. Factors of safety and critical failure surfaces for the slope cases in Figure 22 obtained with FLAC and SLIDE.

computing an impractical large number of models for the development of the computational tools in this paper.

The adoption of the limit equilibrium software SLIDE and the Bishop's method to develop the computational tools in this paper was due to practical reasons mainly. As discussed in the introduction Section 1, the limit equilibrium method is still the most popular method for slope stability analysis due to simplicity and low computer demand, and thousands of models needed to be generated and computed in a reasonable amount of time —the Bishop's formulation was also a natural choice in view of being the least computer intensive formulation of the method of slices. The computational tools could have been developed with some other methods, for example with *limit analysis* methods and/or possibly with any of the *full numerical analysis* methods listed in Table 1, using the shear strength reduction technique —although in the latter case, an impractical amount of time would have been required to compute and process all models needed to develop these tools. A similar comment applies to the critical

failure surface of circular geometry adopted for the limit equilibrium models used to the develop the computational tools. Authors have reported the advantages of using *log-spiral* failure surfaces over circular ones, and particularly the advantages the limit analysis method over the limit equilibrium method [51, 62, 63]. For assumed homogeneous and isotropic rock masses as considered in this paper, the commercial implementations of the limit equilibrium method used in the practice of rock mechanics mining (as listed in Table 1) currently do not allow the analysis of log-spiral failure surfaces, and the (geometrically) circular failure surface is the default one provided for homogeneous isotropic materials in these software implementations. Also, the author is not aware of any commercially available limit analysis software used in the field of rock mechanics mining —although he considers that rock mechanics mining would benefit by the introduction of some commercially available limit analysis software, having similar capabilities as the limit equilibrium ones that are currently available.

For the simple slope cases considered in this paper, no significant differences in values of factor of safety may be expected from application of the computational tools in this paper and more sophisticated methods, like the shear strength reduction technique. Indeed, the similarity of factors of safety from limit equilibrium and limit analysis methods has been discussed and confirmed by several authors in the past —see, for example, [30, 62, 64, 65]; in particular, see [40] for a rigorous mathematical proof of why the similarity holds.

The similarity of factors of safety has also been confirmed with the examples discussed in Section 4, when the limit equilibrium results obtained with the software SLIDE were compared with those obtained with the shear strength reduction technique in the software FLAC. With this regard, it must also be said that despite the similarity of factor of safety results, the example in Section 4.4 put in evidence that the natural shape of the failure surface given by the shear strength reduction technique is not generally geometrically circular. This suggests that a purely geometrically circular shape, adopted as the default one in limit equilibrium software for assumed homogeneous/isotropic material, may be too restrictive. A default shape of the critical failure surface that allows more degrees of freedom in modelling curvature (e.g., a log-spiral shape as mentioned earlier on) may be a good choice for developers of limit equilibrium software, as listed in Table 1, to consider for improvements.

In any case, it must also be emphasized that due to the non-existence of a rigorous closed-form (exact) solution for the simplified slope problem introduced in Section 3 (Figure 7), all of the methods available to perform stability analyses, as listed in Table 1, will be expected to give *approximate* solutions to the problem only. Minor differences in results will always exist when comparing results from different methods, and no one of these methods can be said to be the correct one: they all give approximate results for a problem that has no exact solution.

Finally, understanding that results obtained with the computational tools in this paper are approximate in nature, caution must be exercised when applying these computational tools or any of the software implementations listed in Table 1. In all cases, sound design of slopes in rock masses should be also based on sound engineering judgement and experience.

6. Downloading the computational tools

The computational tools discussed in this paper have been presented originally in the three publications written by the author and colleagues. Pre-print versions of the publications and EXCEL spreadsheets that accompany the publications can be downloaded for free using the links below:

Publication 1: *'Computational tools for the determination of factor of safety and location of the critical failure surface for slopes in Mohr-Coulomb dry ground'* —see [35]; available for downloading at www.d.umn.edu/ carranza/SLOPE18

Publication 2: *'Computational tools for the estimation of factor of safety and location of the critical failure surface for slopes in rock masses that satisfy the Hoek-Brown failure criterion'* —see [36]; available for downloading at www.d.umn.edu/ carranza/SLOPE20

Publication 3: *'Computational tools for the analysis of stability of embankments in frictional-cohesive soils'* —see [37]; available for downloading at www.d.umn.edu/ carranza/EMBK20

References

[1] Read J and Stacey P 2009 *Guidelines for open pit slope design* (CSIRO Publishing. Melbourne, Australia)
[2] Martin C D and Stacey P 2013 *Guidelines for open pit slope design in weak rocks* (CSIRO Publishing. Melbourne, Australia)
[3] Beale G and Read J 2013 *Guidelines for evaluating water in pit slope stability* (CSIRO Publishing. Melbourne, Australia)
[4] Hawley M and Cunning J 2017 *Guidelines for mine waste dump and stockpile design* (CSIRO Publishing. Melbourne, Australia)
[5] Hoek E and Bray J 1974, 1977, 1981 *Rock slope engineering* (Institution of Mining and Metallurgy. London. First, second and third editions, respectively)
[6] Wyllie D C and Mah C 2004 *Rock slope engineering. Civil and Mining* 4th ed (CRC Press)
[7] Wyllie D C 2018 *Rock slope engineering. Civil Applications* (CRC Press. Taylor & Francis)
[8] Coates D F 1967 The stability of slopes in open pits *Proceedings of the 8th Commonwealth Mining and Metallurgical Congress, Australia and New Zealand, 1965-1967* vol 6 (Australasian Institute of Mining and Metallurgy. Melbourne) pp 543–550
[9] Skempton A W and Hutchinson J 1969 Stability of natural slopes and embankment foundations *Proceedings of the 7th International Conference on Soil Mechanics and Foundation Engineering. Mexico City* (Sociedad Mexicana de Mecánica de Suelos)
[10] Varnes D J 1978 Slope movement types and processes *Transportation Research Board Special Report* **176** 11–33
[11] Abramson L W, Lee T S, Sharma S, M G and Boyce 2002 *Slope stability and stabilization methods* 2nd ed (John Wiley & Sons. New York)
[12] Goodman R E 1989 *Introduction to rock mechanics* vol 2 (Wiley)
[13] Giani G P 1992 *Rock slope stability analysis* (Balkema)
[14] Kliche C A 2018 *Rock slope stability* 2nd ed (Society for Mining, Metallurgy, and Exploration, Inc., Littleton, Colorado)
[15] Hoek E and Brown E T 1980 Empirical strength criterion for rock masses *Journal of the Geotechnical Engineering Division ASCE* **106** 1013–1035
[16] Hoek E, and Brown E T 1997 Practical estimates of rock mass strength *International Journal of Rock Mechanics and Mining Sciences* **34** 1165–1186
[17] Hoek E and Brown E T 2019 The Hoek-Brown failure criterion and GSI – 2018 edition *Journal of Rock Mechanics and Geotechnical Engineering* **11** 445–463
[18] Hoek E, Read J, Karzulovic A and Chen Z Y 2000 Rock slopes in civil and mining engineering *Proceedings of GeoEng 2000. International Conference on Geotechnical and Geological Engineering. Melbourne. November 19–24, 2000* pp 643–658
[19] Hormazabal E, Veramendi R, Barrios J, Zuñiga G and Gonzalez F 2013 Slope design at Cuajone Pit, Peru *Proceedings of the International Symposium Slope Stability 2013* (Australian Centre for Geomechanics)
[20] Martin C D and Stacey P 2013 Pit slopes in weathered and weak rocks *Proceedings of the International Symposium Slope Stability 2013* (Australian Centre for Geomechanics) pp 3–28
[21] Sjoberg J 2000 Failure mechanisms for high slopes in hard rock *Slope Stability in Surface Mining* ed Hustrulid et al pp 71–80 Society for Mining, Metallurgical and Exploration (SME). Littleton, Colorado
[22] Steffen O K H, Contreras L F, Terbrugge P J and Others 2008 A risk evaluation approach for pit slope design *The 42nd US Rock Mechanics Symposium (USRMS)* (American Rock Mechanics Association. ARMA)
[23] Coduto D P, Yeung M C and Kitch W A 2011 *Geotechnical engineering. Principles and practices* 2nd ed (Pearson)
[24] Verruijt A 2012 *Soil Mechanics* (Delft University of Technology, Delft, The Netherlands. Available for free dowloading at http://geo.verruijt.net/)
[25] Duncan J M, Wright S G and Brandon T L 2014 *Soil strength and slope stability* (John Wiley & Sons)
[26] Das B M and Sobhan K 2018 *Principles of geotechnical engineering* 9th ed (Cengage)
[27] Bishop A W 1955 The use of the slip circle in the stability analysis of slopes *Géotechnique* **5** 7–17
[28] Matsui T and San K C 1992 Finite element slope stability analysis by shear strength reduction technique *Soils and foundations* **32** 59–70
[29] Griffiths D V and Lane P A 1999 Slope stability analysis by finite elements *Géotechnique* **49** 387–403
[30] Dawnson E M, Roth W H and Drescher A 1999 Slope stability analysis by strength reduction *Géotechnique* **49** 835–840
[31] Hormazabal E, Rovira F, Walker M and Carranza-Torres C 2009 Analysis and design of slopes for Rajo Sur, an open pit mine next to the subsidence crater of El Teniente mine in Chile *Proceedings of the International Symposium Slope Stability 2009. November 9-11, 2009* (Santiago. Chile)
[32] Rocscience Inc 2018 *SLIDE 2018. Slope stability analysis software based on the limit equilibrium method* (Toronto, Canada)

[33] Itasca Consulting Group, Inc 2016 *FLAC (Fast Lagrangian Analysis of Continua) Version 8.0* (Minneapolis, Minnesota)
[34] Microsoft 2016 *EXCEL (software). Version 2016* (Microsoft. Redmond, Washington)
[35] Carranza-Torres C and Hormazabal E 2018 Computational tools for the estimation of factor of safety and location of the critical failure surface for slopes in Mohr-Coulomb dry ground *Proceedings of the 2018 International Symposium on Slope Stability in Open Pit Mining and Civil Engineering. Sevilla, Spain, April 11–13, 2018* (Australian Centre for Geomechanics)
[36] Carranza-Torres C and Hormazabal E 2020 Computational tools for the estimation of factor of safety and location of the critical failure surface for slopes in rock masses that satisfy the Hoek-Brown failure criterion *Proceedings of the 2020 International Symposium on Slope Stability in Open Pit Mining and Civil Engineering. Perth, Australia, May 12-14, 2020* (Australian Centre for Geomechanics) pp 1099–1122
[37] Carranza-Torres C and Saftner D 2020 Computational tools for the analysis of stability of embankments in frictional-cohesive soils *Proceedings of the University of Minnesota 68th Annual Geotechnical Engineering Conference. Minneapolis, Minnesota. February 27, 2020* (Minnesota Geotechnical Society)
[38] Hoek E, Carranza-Torres C and Corkum B 2002 Hoek-Brown failure criterion – 2002 edition *Proceedings of NARMS-TAC 2002, Mining Innovation and Technology. Toronto. July 10, 2002* (University of Toronto) pp 267–273
[39] Jaeger J C, Cook N G W and Zimmerman R 2007 *Fundamentals of rock mechanics* 4th ed (Blackwell Publishing)
[40] Davis R O and Selvadurai A P 2005 *Plasticity and geomechanics* (Cambridge University Press)
[41] Marsal R J 1967 Large scale testing of rockfill materials *Journal of the Soil Mechanics and Foundations Division ASCE* **93** 27–43
[42] Marachi N D, Chan C K and Seed H B 1972 Evaluation of properties of rockfill materials *Journal of the Soil Mechanics and Foundations Division ASCE* **98** 95–114
[43] Indraratna B, Wijewardena L S S and Balasubramaniam A S 1993 Large-scale triaxial testing of grey wacke rockfill *Géotechnique* **43** 37–51
[44] Balmer G 1952 A general analytical solution for Mohr's envelope *Am. Soc. Test. Mat.* 1260–1271
[45] Carranza-Torres C 2004 Some comments on the application of the Hoek-Brown failure criterion for intact rock and rock masses to the solution of tunnel and slope problems *MIR 2004 - X Conference on Rock and Engineering Mechanics. Politecnico di Torino. Turin, Italy. November 2004* ed Barla G and Barla M (Patron Editore. Bologna) pp 285–326
[46] Rocscience Inc 2015 *ROCDATA Version 6. Analysis of rock and soil strength data* (Toronto, Canada)
[47] Carranza-Torres C and Fairhurst C 1999 The elasto-plastic response of underground excavations in rock masses that satisfy the Hoek-Brown failure criterion *International Journal of Rock Mechanics and Mining Sciences* **36** 777–809
[48] Carranza-Torres C and Fairhurst C 2000 Application of the convergence-confinement method of tunnel design to rock masses that satisfy the Hoek-Brown failure criterion *Tunnelling and Underground Space Technology* **15** 187–213
[49] Rose N D, Scholz M, Burden J, King M, Maggs C and Havaej M 2018 Quantifying transitional rock mass disturbance in open pit slopes related to mining excavation *Proceedings of the International Symposium Slope Stability 2018. April 11-13, 2018* (Sevilla. Spain)
[50] Bell J M 1966 Dimensionless parameters for homogeneous earth slopes *Journal of Soil Mechanics & Foundations Div. ASCE* **5** 51–65
[51] Michalowski R L 2002 Stability charts for uniform slopes *Journal of Geotechnical and Geoenvironmental Engineering ASCE* **128-4** 351–355
[52] Baker R 2003 A second look at Taylor's stability chart *Journal of Geotechnical and Geoenvironmental Engineering ASCE* **129** 1102–1108
[53] Steward T, Sivakugan N, Shukla S K and Das B M 2010 Taylor's slope stability charts revisited *International Journal of Geomechanics* **11** 348–352
[54] Itasca Consulting Group, Inc 2017 *FLAC3D (Fast Lagrangian Analysis of Continua in 3 Dimensions) Version 6.0* (Minneapolis, Minnesota)
[55] Hammah R E, Yacoub T E, Corkum B C and Curran J H 2005 The shear strength reduction method for the generalized Hoek-Brown criterion *Proceedings of ARMA/USRM 2005. 40th US Rock Mechanics Symposium: Rock Mechanics for Energy, Mineral and Infrastructure Development in the Northern Regions* (Anchorage, Alaska)
[56] Rocscience Inc 2019 *RS2 2019. Software for geotechnical 2D finite element analysis* (Toronto, Canada)
[57] Harr M E 1991 *Groundwater and seepage* (Dover Publictations, Inc.)
[58] Vanmarcke E H 1980 Probabilistic stability analysis of earth slopes *Engineering Geology* **16** 29–50
[59] Juang C H, Jhi Y Y and Lee D H 1998 Stability analysis of existing slopes considering uncertainty *Engineering Geology* **49** 111–122
[60] Contreras L F and Brown E T 2019 Slope reliability and back analysis of failure with geotechnical parameters estimated using Bayesian inference *Journal of Rock Mechanics and Geotechnical Engineering* **11** 628–643
[61] Lacasse S, Nadim F, Liu Z Q, Eidsvig U K, Le T M H and Lin C G 2019 Risk assessment and dams. Recent developments and applications *Proceedings of the XVII European Conference on Soil Mechanics and Geotechnical Engineering (ECSMGE-2019). Geotechnical Engineering foundation of the future.* Reykjavik, Iceland. September 2019
[62] Yu H S, Salgado R, Sloan S W and Kim J M 1998 Limit analysis versus limit equilibrium for slope stability *Journal of*

Geotechnical and Geoenvironmental Engineering ASCE **124** 1–11
[63] Utili S 2013 Investigation by limit analysis on the stability of slopes with cracks *Géotechnique* **6** 140–154
[64] Cheng Y M, Lansivaara T and Wei W B 2007 Two-dimensional slope stability analysis by limit equilibrium and strength reduction methods *Computers and Geotechnics* **34** 137–150
[65] Leshchinsky B 2013 Comparison of limit equilibrium and limit analysis for complex slopes *Geo-Congress 2013: Stability and Performance of Slopes and Embankments III* pp 1280–1289